REPORT DOCUMENTATION PAGE

Form Approved OMB NO. 0704-0188

1. REPORT DATE (DD-MM-YYYY)	2. REPORT TYPE	3. DATES COVERED (From - To)
23-07-2013	Final Report	1-May-2010 - 30-Apr-2013

4. TITLE AND SUBTITLE

Characterization of Ignition and Combustion Properties of Nanowire-based Energetics

5a. CONTRACT NUMBER
W911NF-10-1-0106

5b. GRANT NUMBER

5c. PROGRAM ELEMENT NUMBER
611102

6. AUTHORS
Xiaolin Zheng

5d. PROJECT NUMBER

5e. TASK NUMBER

5f. WORK UNIT NUMBER

7. PERFORMING ORGANIZATION NAMES AND ADDRESSES
Stanford University
Office of Sponsor Research
Board of Trustees of the Leland Stanford Junior University
Stanford, CA 94305 -4100

8. PERFORMING ORGANIZATION REPORT NUMBER

9. SPONSORING/MONITORING AGENCY NAME(S) AND ADDRESS(ES)
U.S. Army Research Office
P.O. Box 12211
Research Triangle Park, NC 27709-2211

10. SPONSOR/MONITOR'S ACRONYM(S)
ARO

11. SPONSOR/MONITOR'S REPORT NUMBER(S)
57416-EG.6

12. DISTRIBUTION AVAILIBILITY STATEMENT
Approved for Public Release; Distribution Unlimited

13. SUPPLEMENTARY NOTES
The views, opinions and/or findings contained in this report are those of the author(s) and should not contrued as an official Department of the Army position, policy or decision, unless so designated by other documentation.

14. ABSTRACT
This research program focused on the ignition properties of nanoscale energetic materials made of Al and metal oxides. We made contributions in three frontiers of energetic materials: 1) demonstrating that core/shell morphology leads to high activity due to uniform mixing between fuels and oxidizers; 2)innovating the first application of flash ignition of Al nanoparticles and micron particles; and 3) realizing flash ignition of porous Si film and elucidating the effects of film thickness and porosity on the minimum ignition energy.

15. SUBJECT TERMS

16. SECURITY CLASSIFICATION OF:			17. LIMITATION OF ABSTRACT	15. NUMBER OF PAGES	19a. NAME OF RESPONSIBLE PERSON
a. REPORT	b. ABSTRACT	c. THIS PAGE			Xiaolin Zheng
UU	UU	UU	UU		19b. TELEPHONE NUMBER 650-736-8953

Report Title

Characterization of Ignition and Combustion Properties of Nanowire-based Energetics

ABSTRACT

This research program focused on the ignition properties of nanoscale energetic materials made of Al and metal oxides. We made contributions in three frontiers of energetic materials: 1) demonstrating that core/shell morphology leads to high activity due to uniform mixing between fuels and oxidizers; 2)innovating the first application of flash ignition of Al nanoparticles and micron particles; and 3) realizing flash ignition of porous Si film and elucidating the effects of film thickness and porosity on the minimum ignition energy.

Enter List of papers submitted or published that acknowledge ARO support from the start of the project to the date of this printing. List the papers, including journal references, in the following categories:

(a) Papers published in peer-reviewed journals (N/A for none)

Received		Paper
06/30/2011	1.00	Y. Ohkura, P. Rao, X. Zheng. Flash Ignition of Al Nanoparticles: Mechanism and Applications, The Combustion Institute, (05 2011): . doi:
07/23/2013	5.00	Yuma Ohkura, Pratap M. Rao, In Sun Cho, Xiaolin Zheng. Reducing minimum flash ignition energy of Al microparticles by addition of WO3 nanoparticles, Applied Physics Letters, (01 2013): 0. doi: 10.1063/1.4790152
TOTAL:	**2**	

Number of Papers published in peer-reviewed journals:

(b) Papers published in non-peer-reviewed journals (N/A for none)

Received		Paper
07/23/2013	4.00	Yuma Ohkura, Jeffrey M. Weisse, Xiaolin Zheng. Flash Ignition of Freestanding Porous SiliconFilm: Effects of Film Thickness and Porosity, Under preparation, (08 2013): 0. doi:
08/22/2012	2.00	Yuma Ohkura, Shih-Yu Liu, Pratap M. Rao, Xiaolin Zheng. Synthesis and ignition of energetic CuO/Al core/shell nanowires, Proceedings of the Combustion Institute, (08 2010): 1909. doi:
TOTAL:	**2**	

Number of Papers published in non peer-reviewed journals:

(c) Presentations

Number of Presentations: 0.00

Non Peer-Reviewed Conference Proceeding publications (other than abstracts):

Received Paper

TOTAL:

Number of Non Peer-Reviewed Conference Proceeding publications (other than abstracts):

Peer-Reviewed Conference Proceeding publications (other than abstracts):

Received Paper

TOTAL:

Number of Peer-Reviewed Conference Proceeding publications (other than abstracts):

(d) Manuscripts

Received Paper

TOTAL:

Number of Manuscripts:

Books

Received	Paper

TOTAL:

Patents Submitted

Y. Ohkura and X. L. Zheng, "Optical Ignition of Fuels," Provisional patent application (61/773,953).

Patents Awarded

.Y. Ohkura and X. L. Zheng, "Distributed Ignition Of Fuels Using Nanoparticles," US 2012-051931.

Awards

TechConnect National Innovation Award, TechConnect-National Innovation Summit, 2013
3M Nontenured Faculty Grant Award, 2013

Graduate Students

NAME	PERCENT_SUPPORTED	Discipline
Yuma Ohkura	1.00	
Pratap M. Rao	1.00	
FTE Equivalent:	**2.00**	
Total Number:	**2**	

Names of Post Doctorates

NAME	PERCENT_SUPPORTED
FTE Equivalent:	
Total Number:	

Names of Faculty Supported

NAME	PERCENT_SUPPORTED	National Academy Member
Xiaolin Zheng	0.01	
FTE Equivalent:	**0.01**	
Total Number:	**1**	

Names of Under Graduate students supported

NAME	PERCENT_SUPPORTED
FTE Equivalent:	
Total Number:	

Student Metrics

This section only applies to graduating undergraduates supported by this agreement in this reporting period

The number of undergraduates funded by this agreement who graduated during this period:	0.00
The number of undergraduates funded by this agreement who graduated during this period with a degree in science, mathematics, engineering, or technology fields:.....	0.00
The number of undergraduates funded by your agreement who graduated during this period and will continue to pursue a graduate or Ph.D. degree in science, mathematics, engineering, or technology fields:.....	0.00
Number of graduating undergraduates who achieved a 3.5 GPA to 4.0 (4.0 max scale):	0.00
Number of graduating undergraduates funded by a DoD funded Center of Excellence grant for Education, Research and Engineering:	0.00
The number of undergraduates funded by your agreement who graduated during this period and intend to work for the Department of Defense	0.00
The number of undergraduates funded by your agreement who graduated during this period and will receive scholarships or fellowships for further studies in science, mathematics, engineering or technology fields:	0.00

Names of Personnel receiving masters degrees

NAME
Andrew Liu
Total Number: 1

Names of personnel receiving PHDs

NAME
Pratap M. Rao
Total Number: 1

Names of other research staff

NAME	PERCENT_SUPPORTED
FTE Equivalent:	
Total Number:	

Sub Contractors (DD882)

Inventions (DD882)

5 **Distributed Ignition Of Fuels Using Nanoparticles**

Patent Filed in US? (5d-1) Y

Patent Filed in Foreign Countries? (5d-2) N

Was the assignment forwarded to the contracting officer? (5e) N

Foreign Countries of application (5g-2):

5a: Y. Ohkura and X. L. Zheng

5f-1a: Stanford University

5f-c: 452 Escondido Mall

Stanford CA 94305

5 **Optical Ignition of Fuels**

Patent Filed in US? (5d-1) Y

Patent Filed in Foreign Countries? (5d-2) N

Was the assignment forwarded to the contracting officer? (5e) N

Foreign Countries of application (5g-2):

5a: Y. Ohkura and X. L. Zheng

5f-1a: Stanford University

5f-c: 452 Escondido Mall

Stanford CA 94305

Scientific Progress

Technology Transfer

Final Report:

Characterization of Ignition and Combustion Properties of Nanowire-based Energetics

Xiaolin Zheng
Department of Mechanical Engineering,
Stanford University, Stanford, CA 94305

Grant No.: W911NF-10-0106

Submitted to: Department of the Army

Report coverage: 05/01/2010 – 04/30/2013

Executive Summary

This research program focused on the ignition properties of nanoscale energetic materials made of Al and metal oxides. We made contributions in three frontiers of energetic materials: 1) demonstrating that core/shell morphology leads to high activity due to uniform mixing between fuels and oxidizers; 2) innovating the first application of flash ignition of Al nanoparticles and micron particles; and 3) realizing flash ignition of porous Si film and elucidating the effects of film thickness and porosity on the minimum ignition energy.

We have first investigated the morphology effect on ignition of nanoscale energetic materials. Specifically, we successfully synthesized thermites with a new nanostructure, i.e., CuO/Al core/shell nanowires (NWs) and characterized their ignition processes by thermal differential scanning calorimetry. The CuO NW cores were synthesized by the thermal annealing of copper films and served as templates for the deposition of Al shells by subsequent sputtering. The advantage of such a core/shell NW structure is that CuO and Al are uniformly mixed at the nanoscale. The onset temperatures of the exothermic reaction of the core/shell NWs were similar to those of nanoparticle (NP)-based thermites in terms of magnitude, insensitivity to equivalence ratios and sensitivity to heating rates. Moreover, the core/shell NW thermites, compared to NP-based thermites, exhibit greatly improved mixing uniformity and reduced activation energy for the thermite reaction. A description of these experiments is given in the attached reprint.

- *"Synthesis and Ignition of Energetic CuO/Al Core/Shell Nanowires", Y. Ohkura, S. Y. Liu, P. M. Rao and* ***X. L. Zheng****,* ***Proc. Combust. Inst.*** *33, 1909-1915 (2011).*

Next, we invented a simple, distributed, optical ignition method that uses a millisecond exposure of a camera flash to ignite Al nanoparticles (NPs) to Al micron particles (MPs). We demonstrated for the first time that Al NPs can be used as a primer to ignite energetic Al/CuO mixture, heptane and methane upon exposure of a camera flash. Our analysis suggests that successful flash ignition requires suitable diameters and high packing density of Al NPs to have high enough temperature rise beyond their ignition temperatures. Significantly, transmission electron microscopy analysis reveals that Al NPs are oxidized through the melt-dispersion mechanism. The flash ignition of Al NPs is due to the photothermal effect, which is very challenging for Al MPs because have smaller light absorption due to increased light scattering and simultaneous higher ignition temperatures. Flash ignition of Al MPs was achieved previously but with very high-power xenon flash lamps (around or above 25 J/cm^2). We realized a successful low-power (1 J/cm^2) flash ignition of Al MPs by addition of WO_3 nanoparticles (NPs). We believe that the main roles of WO_3 NPs in facilitating Al MPs flash ignition is to increase light absorption and effectively supply oxygen due to their large specific surface area as well as their close contact with Al MPs for the following reasons. Detailed description of flash ignition of Al particles are given in the attached reprints.

- *"Reducing Minimum Flash Ignition Energy of Al Microparticles by Addition of WO_3 Nanoparticles", Y. Ohkura, P. M. Rao, I. S. Cho and* ***X. L. Zheng, Applied Physics Letters,*** *102, 043108 (2013).*

- *"Flash Ignition of Al Nanoparticles: Mechanism and Applications", Y. Ohkura, P. M. Rao, and* ***X. L. Zheng, Combustion and Flames****, 158, 2544-2548 (2011).*

Finally, we successfully extended flash ignition from Al particles to porous silicon (Si). Porous Si is an emerging materials for and pyrotechnic applications. We realized the first flash ignition of freestanding porous Si films in air with no additional oxidizers. We conducted high speed camera imaging, energy-dispersive X-ray spectroscopy, X-ray diffraction, and thermogravimetric analysis to understand the flash ignition process. Our experiments and simulations reveal that the minimum flash ignition energies are sensitive to film thickness and porosity, due to the coupled effects of light absorption, heat conduction and heat capacity. A description of these experiments is given in the attached manuscript.

- *"Flash Ignition of Freestanding Porous Silicon Film: Effects of Film Thickness and Porosity", Y. Ohkura, J. M. Weisse, and X. L. Zheng, in preparation.*

Other Accomplishments

1. Awards received and nominations

- TechConnect National Innovation Award, TechConnect-National Innovation Summit, 2013
- 3M Nontenured Faculty Grant Award, 2013

2. ALL Dissemination with ONR Support: papers, articles, journals, and books.

Journal Papers

(1) "Flash Ignition of Freestanding Porous Silicon Film: Effects of Film Thickness and Porosity", Y. Ohkura, J. M. Weisse, and X. L. Zheng, in preparation.

(2) "Reducing Minimum Flash Ignition Energy of Al Microparticles by Addition of WO_3 Nanoparticles", Y. Ohkura, P. M. Rao, I. S. Cho and **X. L. Zheng,** ***Applied Physics Letters,*** 102, 043108 (2013).

(3) "Flash Ignition of Al Nanoparticles: Mechanism and Applications", Y. Ohkura, P. M. Rao, and **X. L. Zheng,** ***Combustion and Flames***, 158, 2544-2548 (2011).

(4) "Synthesis and Ignition of Energetic CuO/Al Core/Shell Nanowires", Y. Ohkura, S. Y. Liu, P. M. Rao and **X. L. Zheng**, ***Proc. Combust. Inst.*** *33*, 1909-1915 (2011).

Conference Presentations

(1) "Synthesis and Ignition of Energetic CuO/Al Core/Shell Nanowires", *the 33rd International Symposium on Combustion*, Beijing, China, 2010.

(2) "Flash ignition of Al Nanoparticles: Applications and mechanism", *Thermal & Fluid Sciences Affiliates and Sponsors Conference*, Stanford, USA, 2011.

(3) "Flash ignition of Al particles", *MRS Fall Meeting*, Boston, USA, 2011.

(4) "Reducing minimum flash ignition energy of Al microparticles by addition of WO_3 nanoparticles", *MRS Fall Meeting*, Boston, USA, 2012.

(5) "Reducing minimum flash ignition energy of Al microparticles by addition of WO_3 nanoparticles", *the 8th U.S. National Combustion Meeting*, Park City, USA, 2013.

3. Names of all supported students and post docs.

- Dr. Pratap M. Rao, Graduated in 2013, Assistant Professor at Worcester Polytechnic Institute
- Yuma Ohkura, 5th graduate student, expected to receive his PhD in September.

Available online at www.sciencedirect.com
ScienceDirect
Proceedings of the Combustion Institute 33 (2011) 1909–1915
Proceedings of the Combustion Institute
www.elsevier.com/locate/proci

Synthesis and ignition of energetic CuO/Al core/shell nanowires

Yuma Ohkura, Shih-Yu Liu, Pratap M. Rao, Xiaolin Zheng *

Department of Mechanical Engineering, Stanford University, Stanford, CA 94305, United States

Available online 6 August 2010

Abstract

Energetic thermites (mixtures of Al and metal oxides), due to their high energy densities, have broad applications in propulsion, thermal batteries, waste disposal, and power generation for micro systems. Reducing the sizes of Al and metal oxides down to the nanoscale has been shown to be effective in increasing their reaction rates and reducing their ignition delays. However, it remains a challenge to create mixtures of Al and metal oxides with nanoscale uniformity. Here we report synthesis and ignition studies on thermites with a new nanostructure, i.e., CuO/Al core/shell nanowires (NWs). The CuO NW cores were synthesized by the thermal annealing of copper films and served as templates for the deposition of Al shells by subsequent sputtering. The advantage of such a core/shell NW structure is that CuO and Al are uniformly mixed at the nanoscale. The onset temperatures of the exothermic reaction of the core/shell NWs were similar to those of nanoparticle (NP)-based thermites in terms of magnitude, insensitivity to equivalence ratios and sensitivity to heating rates. Moreover, the core/shell NW thermites, compared to NP-based thermites, exhibit greatly improved mixing uniformity and reduced activation energy for the thermite reaction.

Keywords: Nanoenergetic materials; Thermite; Nanowire; CuO/Al core/shell nanowire; Ignition

1. Introduction

Energetic thermites (mixtures of Al and metal oxides), due to their high energy densities and capacity for self-sustained reaction, are extremely energy efficient, and have broad practical applications ranging from propulsion, thermal batteries, material synthesis, waste disposal to power generation for micro systems [1–5]. However, one of the major limitations of thermites as energetic materials is their long ignition delay times [6]. Reducing the sizes of Al and metal oxide particles to the nanoscale has been demonstrated to be effective in facilitating the ignition process [7,8]. For example, Pantoya and Granier [9] have shown that the onset temperature of Al/MoO_3 composites was reduced by at least 300 °C when the Al particle size was decreased from several microns to below 100 nm. Pantoya and Granier [10] have also demonstrated that the ignition delay time of Al/MoO_3 composites using laser ignition was reduced from 1384 ms to around 20 ms by decreasing the average Al particle size from 10 μm to below 200 nm. Similarly, Brandstadt et al. [11] have shown that the onset temperature of the oxidation of Al in CO_2 decreased from around 920–940 °C to 500–510 °C while the Al particle size was reduced from 10 μm to 38 nm. In addition, nanoscale Al/MoO_3

* Corresponding author. Fax: +1 650 723 1748.
E-mail address: xlzheng@stanford.edu (X. Zheng).

1540-7489/$ - see front matter © 2010 The Combustion Institute. Published by Elsevier Inc. All rights reserved.
doi:10.1016/j.proci.2010.05.048

thermites were demonstrated to have burning rates ranging from 600–1000 m/s in an open-ended acrylic tube, which is 1000 times faster than the micron size thermites [12–14].

These nanoscale thermites (or nano-thermites) can be produced by many methods which were summarized in recent reviews [5,7,8,15], such as arrested reactive milling [6,16–19], powder mixing [13,20–22], self-assembly [23,24], and layered vapor deposition [25,26]. However, all of these methods suffer from certain shortcomings. For instance, although the mechanical mixing of Al with metal oxide nanoparticles (NPs), such as direct mixing in an ultrasonic bath using hexane or isopropanol [27], is simple, it cannot homogeneously mix Al and metal oxides with a large degree of spatial homogeneity due to aggregation of the same type of NPs. As such, these materials exhibit large scatter in their ignition and burning characteristics. Moreover, metal oxides synthesized or mixed in the solution phase typically contain hydroxyl groups, water, and hydrocarbons [23], that act as heat sinks by absorbing energy, and hence retard the ignition and flame propagation processes [28]. Blobaum et al. [25,29] demonstrated a different method to form highly uniform CuO_x/Al multilayer foils by alternatively depositing Al and copper oxide layers with well-defined thicknesses under high vacuum, but this fabrication process is costly, time-consuming and difficult to scale up. The above limitations have hindered the fundamental understanding and optimization of nano-thermites. Therefore, there is a critical need to develop new, simple and yet scalable methods to create well-defined thermites with nanoscale mixing and homogeneity for both fundamental studies and practical applications.

Recently, one-dimensional nanowires (NWs) have been used as templates to assemble nano-thermites for improved mixing uniformity. One approach is to coat metal oxide NWs with an adhesive polymer to bond Al NPs onto the sidewalls of NWs [23,24]. The advantage of this approach is that the cylindrical geometry of NWs allows a relatively larger number of Al NPs to be assembled to a single NW. Nevertheless, the attachment of Al NPs to the NWs is not uniform along the axial direction of NWs. Another approach is to directly deposit a layer of Al film with controlled thickness on top of metal oxide NWs to form uniform metal oxide/Al core/shell NW thermites [30,31]. However, studies on the second approach have been focused on the fabrication process for integration of the nano-thermites onto silicon wafers for potential applications in microelectronic mechanical systems. Fundamental ignition characteristics of these core/shell NW thermites were not systematically studied and no comparison with the conventional NP thermites was made.

In view of the above considerations, we have performed experimental determinations of the ignition and heat release characteristics of the CuO/Al core/shell NW thermites in helium environments by using differential scanning calorimetry (DSC). The CuO/Al core/shell NWs were synthesized by the thermal annealing of electroplated Cu film to grow CuO NWs, followed by Al film deposition by sputtering. The onset temperature of the exothermic reaction of the CuO/Al core/shell NWs was measured to be in the range of 550–570 °C, insensitive to the overall equivalence ratios, and to increase with increasing heating rates. The CuO/Al core/shell NW thermites have demonstrated two notable advantages over thermites consisting of CuO NPs and Al NPs: (1) significantly reduced activation energy for the thermite reaction, and (2) greatly improved mixing uniformity.

2. Experimental specifications

The fabrication process of the CuO/Al core/shell NWs is illustrated in Fig. 1. First, a layer of copper film was electroplated over a steel plate using a flash copper™ plating kit (Castwell Inc.) with a current density of 20 mA/cm^2, which yields a deposition rate of approximately 60 nm/min. We deposited a copper film of 1 μm thickness because it gives the optimal CuO NW density with a thin supporting CuO layer. Before electroplating, the steel plate was thoroughly cleaned with acetone, methanol, and isopropyl alcohol, in sequence, to remove any organic impurities and promote the adhesion of copper. Second, CuO NWs were grown by the simple thermal annealing method [32], in which the electroplated copper film was heated on a hotplate at 500 °C for 5 or 24 h under ambient conditions. After annealing, the color of the copper film changed from shiny brown to black (Fig. 1a, inset), indicating that Cu has been oxidized to CuO. Scanning electron microscopy (SEM, FEI XL30 Sirion, 5 kV) imaging (Fig. 1b) shows that CuO NWs have been formed with a perpendicular orientation with respect to the Cu film. Finally, a layer of Al film was deposited over the CuO NWs by magnetron sputtering under a vacuum level of 5×10^{-3} Torr. Magnetron sputtering was selected over other metal deposition techniques, such as electron beam and thermal evaporation, because it provides enhanced conformal coating, resulting in a uniform CuO/Al core/shell NW structure (Fig. 1c and d). Since the deposition rate on the sidewall of NWs is typically smaller than that on a flat surface, the actual thickness of the Al layer was always independently measured by SEM. The Al layer thicknesses analyzed in this paper were set to be 0.5, 1.0, 1.5 μm for a flat surface, and the actual shell thicknesses are around 100, 250, and 425 nm.

The morphology and surface coverage density of the CuO NWs can be easily tuned by varying the annealing temperature and time. For example,

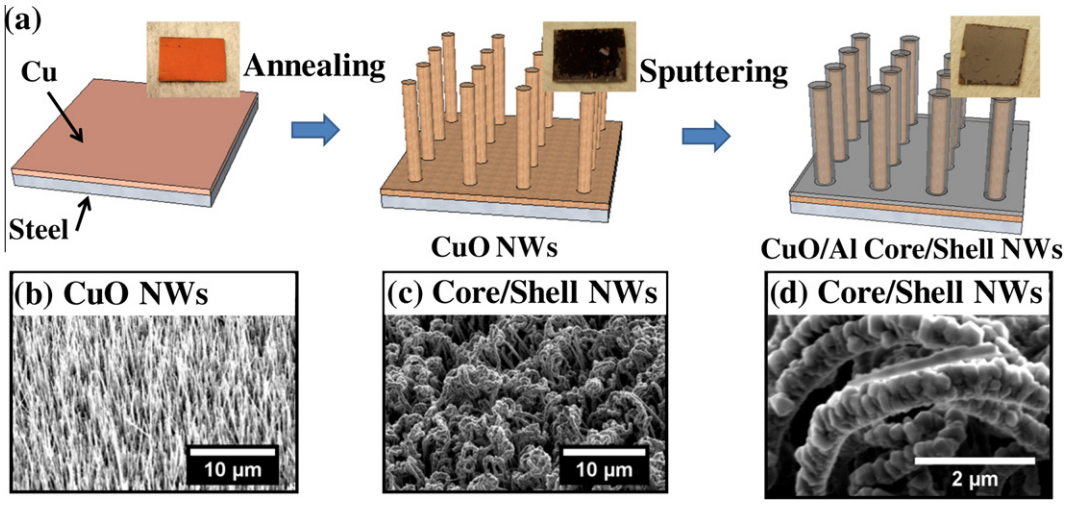

Fig. 1. (a) Schematics of the fabrication process of the CuO/Al core/shell NWs. The insets are the corresponding optical images. SEM images of the (b) CuO NWs, (c) CuO/Al (250 nm) core/shell NWs, and (d) enlarged view of (c).

the CuO NWs grown for 5- and 24-hour annealing were compared in Fig. 2. The average length and diameter of the CuO NWs are 3–7 μm and 40–90 nm for the 5-hour annealing case and 12–16 μm and 50–100 nm for the 24-hour annealing case, respectively. The surface density of NWs for the 24-hour annealing case, estimated on the basis of SEM images (Fig. 2b), is about 10^8–10^9 NWs/cm^2, which is significantly larger than that of the 5-hour annealing case (Fig. 2a). As such, the annealing conditions provide a convenient way to control the amount of CuO loading per unit area for the thermite reaction. All the results reported here were based on the CuO NWs synthesized for 24 h. It should be noted that a CuO layer of approximately 2 μm thickness is formed immediately beneath the CuO NWs during the growth process (Fig. 2b inset) which, together with the CuO NWs, easily separates from the underlying steel plate. The CuO layer cannot be isolated from the CuO NWs, so it is also a part of the thermite sample.

The ignition and heat release characteristics of the energetic CuO/Al core/shell NWs were studied using differential scanning calorimetry (DSC, SETSYS Evolution DTA/DSC). The CuO/Al core/shell NWs were scraped from the steel plate with a razor and placed in an inert alumina crucible during the DSC measurement. Before each test, the DSC chamber was evacuated and flushed twice with inert He gas to remove any residual air. The sample was then heated from room temperature in the DSC furnace under the inert He environment with a controlled heating rate of 5 °C/min between 350 °C and 800 °C, unless otherwise specified. The heat release was calibrated against a standard KBr sample with a known heat of fusion of 216 ± 3 J/g at a melting temperature of 734 °C [33].

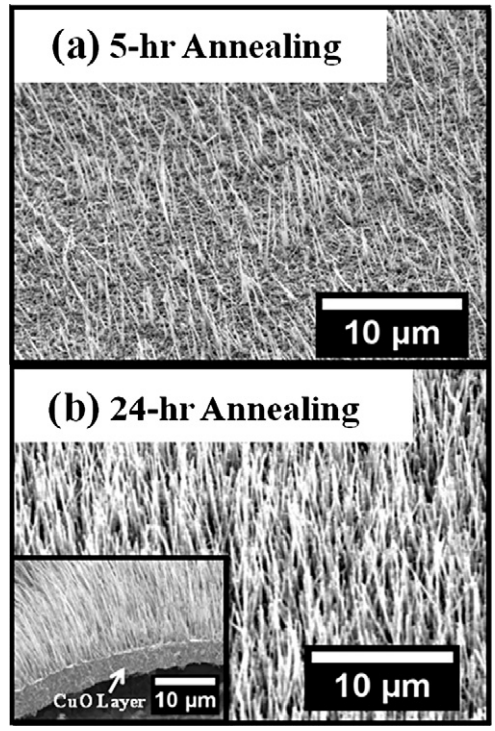

Fig. 2. Effect of the growth time on morphology of the CuO NWs annealed at 500 °C. SEM images of NWs grown for (a) 5 h and (b) 24 h. The inset shows that the CuO NWs are connected to the underneath CuO layer.

The compositions of the tested samples were analyzed by parallel beam X-ray diffraction (XRD, PANalytical XPert 2, Cu $K\alpha$, 45 kV, 40 mA) before and after the DSC measurement. The typical XRD spectra of the initial reactants and

final products are shown in Fig. 3. The XRD spectrum of the initial CuO/Al core/shell NWs, as expected, shows two major crystalline phases, corresponding to CuO and Al, respectively. After the DSC test, the XRD spectrum of the final product exhibits dominant peaks of Cu_2O and smaller peaks of CuO and Al, indicating that CuO has been reduced by Al. The absence of Al_2O_3 peaks is probably due to the fact that the Al_2O_3 product phase is amorphous or poorly crystalline [34].

In addition, we tested commercial CuO NPs and Al NPs in order to compare the differences between NP-based and NW-based thermites. The Al NPs (SkySpring International, Inc.) and the CuO NPs (Inframat Advanced Materials) have average diameters of 70 nm and 60 nm, and densities of 2.7 g/cm^3 and 6.3 g/cm^3, respectively. The CuO/Al NPs mixtures were prepared in different equivalence ratios by manual mixing.

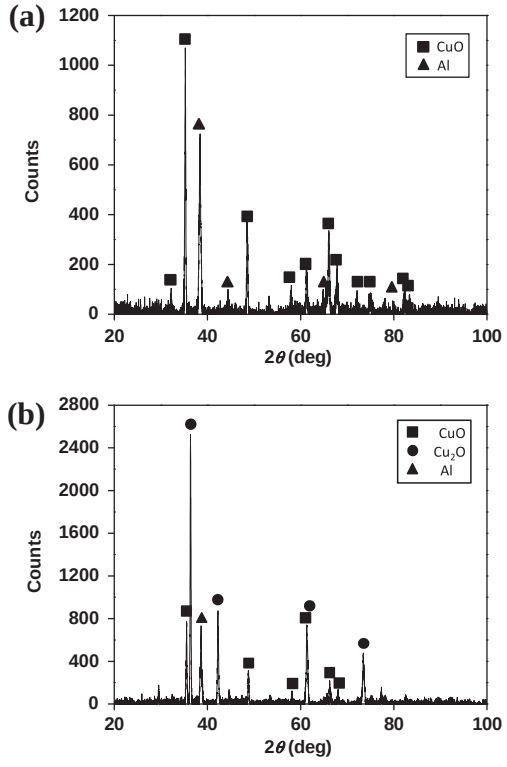

Fig. 3. Parallel beam XRD of CuO/Al (250 nm) core/shell NWs (a) before and (b) after the DSC test. The CuO NWs were annealed at 500 °C for 24 h.

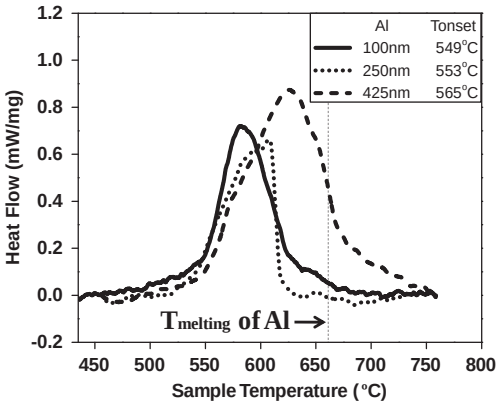

Fig. 4. DSC traces for reactions of the CuO/Al core/shell NWs with different Al shell thickness (100 nm, 250 nm, and 425 nm). All the traces were recorded in inert He at a heating rate of 5 °C/min.

3. Results and discussion

3.1. Effect of the Al layer thickness

Figure 4 shows the effect of the Al layer thickness on the exothermic heat release of the CuO/Al core/shell NWs. The average thicknesses of the Al layer of the three tested samples are 100, 250, and 425 nm, respectively. The exact equivalence ratio of the CuO/Al thermite cannot be calculated accurately because the NWs cannot be cleanly separated from the underlying CuO layer (Fig. 2b inset). Hence, increasing the thickness of the Al layer is a qualitative method to increase the overall fuel/oxidizer equivalence ratio. First of all, the onset temperature of the exothermic thermite reaction, defined as the inflection point ($\frac{d^2q}{dt^2} = 0$) on the rising edge of the heat flow vs. temperature curve and extracted by fitting this part of the curve by a fourth order polynomial, is comparable, in the range of 549–565 °C for all three cases. The exothermic onset temperature of the CuO/Al NWs is below the melting temperature of Al (660 °C) and much lower than the exothermic onset temperature (1040 °C) of micron-sized stoichiometric CuO and Al mixture under the same test conditions. This supports the fact that reducing the dimensions of CuO and Al to the nanoscale can significantly facilitate the ignition process [9]. Second, the exothermic onset temperature of the CuO/Al NWs only increases by about 16 °C when the Al layer thickness is increased by more than four times (Fig. 4). The insensitivity of ignition temperature to the equivalence ratio was also observed previously for the laser ignition of Al/MoO_3 nano-thermites prepared by ultrasonic mixing of respective NPs, for which the ignition delays show little variation over the equivalence ratio range of 0.5–2 [10]. Finally, there was no endothermic peak observed at the melting temperature of Al for any of the three CuO/Al core/shell NWs (Fig. 4), suggesting that there is no Al left unreacted. The endothermic peak has been observed for both CuO/Al NPs and similar CuO/Al core/shell NWs, for which

Al was deposited by thermal evaporation [30]. It indicates that our fabrication method, combining long growth time of CuO NWs and conformal coating of Al with magnetron sputtering, generates spatially-uniform CuO/Al nano-thermite without local accumulation of Al, as observed in the case of mixing NPs.

3.2. Effect of heating rate

The ignition and heat release characteristics of the CuO/Al core/shell NWs with 250 nm thick Al layers were further studied and compared under different heating rates. The effect of heating rate is not only of practical importance because different ignition methods have different heating rates, but also of fundamental interest because the heating rate can affect the reaction mechanism of nano-thermites [9]. First, as shown in Fig. 5a, the heat release profile broadens as the heating rate is increased. This is due to the fact that, under larger heating rates, the sample experiences larger spatial heterogeneity in terms of temperature and the onset of reaction, so the heat release profile tends to be broader and more irregular. Second, no endothermic peak associated with the melting of Al was observed for all the cases with different heating rates, which again supports the fact that Al was coated over the CuO NWs with excellent spatial uniformity without local accumulation. Finally, the exothermic onset temperature of the CuO/Al NWs increases significantly with increasing heating rate, as shown in Fig. 5b, a typical characteristic of the thermal lag due to the larger heating rate. For instance, the exothermic onset temperature is increased by more than 50 °C when the heating rate is increased from 5 °C/min to 40 °C/min, and is far more sensitive to the heating rate than to the equivalence ratio (Fig. 4). Such a strong dependence of the exothermic onset temperature on the heating rate is similar to that of Al/MoO_3 NP thermites reported by Pantoya and Granier [9].

The global activation energy and the pre-exponential A factor of the CuO/Al core/shell NW thermite reaction were extracted on the basis of the Kissinger relation [35,36]:

$$\frac{T_p^2}{\beta} = E_a/(RA)\exp\left(\frac{E_a}{RT_p}\right), \quad (1)$$

where T_p (K) denotes the temperature at which the peak heat release occurs, β the heating rate (°C/s), E_a the activation energy (kJ/mol), R the universal gas constant and A the pre-exponential factor (s^{-1}). Therefore, the activation energy E_a and the A factor can be calculated from the slope and the intercept of the $\ln(T_p^2/\beta)$ vs. $1/T_p$ curve, as shown in Fig. 6. The extracted E_a and A for the CuO/Al core/shell NWs with 250 nm thick Al layer are about 102 kJ/mol and $2.42 \times 10^3\ s^{-1}$.

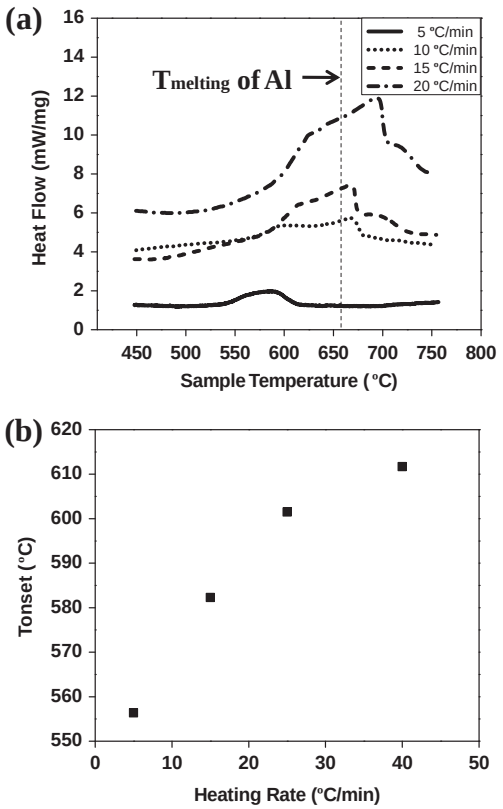

Fig. 5. (a) DSC traces for reactions of the CuO/Al (250 nm) core/shell NWs at heating rates of 5 °C/min, 15 °C/min, 25 °C/min, and 40 °C/min. (b) The exothermic onset temperatures of the CuO/Al core/shell NWs at different heating rates.

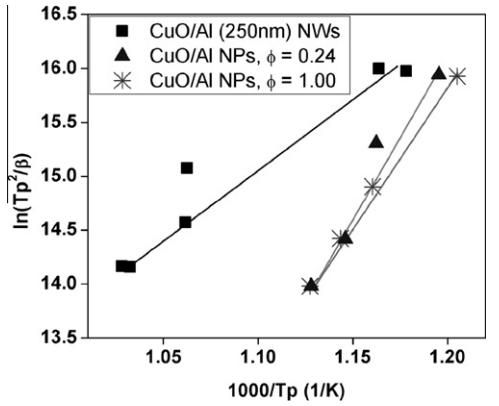

Fig. 6. Thermal analysis of DSC traces for the CuO/Al (250 nm) core/shell NWs, and CuO/Al NPs at equivalence ratios of 1.00 and 0.24. The activation energies of the reacting materials are determined by the slope of the lines.

We also performed the DSC measurements of the mixture of CuO NPs and Al NPs under different heating rates as a comparison. The activation

energies and A factors of the CuO/Al NP thermites are about 250 kJ/mol and 2.96×10^{10} s^{-1}, and 207 kJ/mol and 1.36×10^{13} s^{-1}, and 2.96×10^{10}, 1.36×10^{13} s^{-1} for the equivalence ratio of 0.24 and 1.00, respectively. Although the exact equivalence ratio of the CuO/Al core/shell NWs is unknown, its E_a is almost half of both the fuel-lean and stoichiometric CuO/Al NPs, suggesting that the thermite reaction between CuO and Al in this core/shell NW structure occurs more readily than that in the NP mixtures. One potential reason is that the native Al_2O_3 shell outside the Al NPs has to be melted or broken in order for Al to contact CuO for reaction. However, Al is already in contact with CuO in the core/shell NW structure. Even though there may exist a partially reacted interface between CuO and Al after the deposition of Al, this layer, unlike the outermost Al_2O_3 shell, does not require to be melted or broken for reaction to initiate. Consequently, oxygen only needs to diffuse within the NWs which facilities the reaction of the core-shell NWs.

3.3. Comparison of nanowire- and nanoparticle-based thermites

To further explore the potential of NW-based thermites, we have compared the ignition and heat release behaviors of three samples, *i.e.*, the CuO/Al core/shell NWs (Al thickness: 425 nm), a stoichiometric mixture of CuO NWs and Al NPs (70 nm), and a stoichiometric mixture of CuO NPs (60 nm) and Al NPs (70 nm). All three samples were heated under inert He environments inside the DSC furnace with a heating rate of 5 °C/min, and their typical DSC traces are shown in Fig. 7. First of all, although the heat release profiles of all three samples have well-defined single peaks, the widths of the heat release profiles are much broader for the two samples containing CuO NWs. One possible reason is that the CuO NWs scraped from the steel plate always contain some of the CuO thin film layer (Fig. 2b inset), which reacts with Al at higher temperature compared to the CuO NWs, leading to the broadening of the heat release profile. In other words, the overall reaction proceeds in two steps: CuO NWs first react with Al followed by the reaction between the CuO layer and Al. Second, all three samples have very similar exothermic onset temperatures, 550 °C for the CuO/Al core/shell NWs, 545 °C for the CuO NWs/Al NPs and 540 °C for the CuO NPs/Al NPs, which are below the melting temperature of Al. This suggests that ignition of nano-thermites, regardless of their morphologies and structures, is greatly facilitated by reducing the diffusion length of oxygen. In addition, the CuO film layer seems to have a negligible effect on the exothermic onset temperature, suggesting that ignition is initiated by reaction between the CuO NWs and Al.

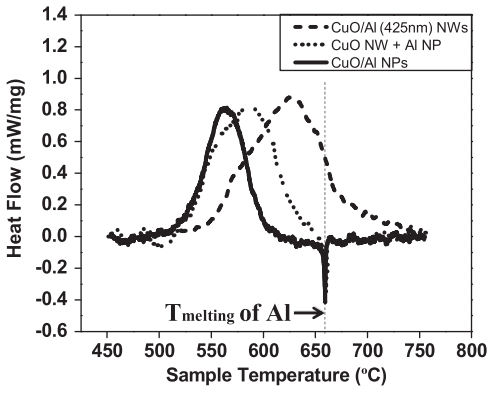

Fig. 7. Comparison of DSC traces for reactions of CuO/Al (425 nm) core/shell NWs, a stoichiometric mixture of CuO NWs and Al NPs, and a stoichiometric mixture of CuO and Al NPs.

More importantly, one distinctive feature of the heat release profile for the CuO/Al core/shell NW sample (Fig. 7) is the lack of the endothermic peak around the melting temperature of Al (660 °C). However, such an endothermic peak, for both the CuO NWs/Al NPs and the CuO NPs/Al NPs samples, appears after the heat flow has leveled off, indicating there are some Al NPs left after the thermite reaction, although both samples are stoichiometric and, in theory, Al should have been totally consumed. Moreover, such endothermic peaks were also observed for fuel-lean CuO NPs/Al NPs samples of equivalence ratio of 0.50 and 0.24 and stoichiometric CuO/Al nanocomposites samples prepared by arrested reactive milling reported by Umbrajkar et al. [34]. It suggests that it is difficult or even impossible to achieve perfect spatial uniformity by mechanically mixing two solid phase components. In other words, there will always be regions of more Al and regions of less Al, so that some Al will be left unreacted. On the contrary, in the case of CuO/Al core/shell NWs, the CuO NWs provide an excellent template for the uniform coating and distribution of Al. Even though the core/shell NWs can be broken into pieces during the sample handling process, each piece is still a uniform CuO/Al mixture so that there is no pocket of Al accumulation and the corresponding endothermic peak. Hence, the current CuO/Al core/shell NW structure significantly improves the overall spatial uniformity of the nano-thermites, and provides an ideal platform for the study of the thermodynamic and kinetic properties of nano-thermites. Finally, the similarities observed for the CuO NWs/Al NPs and the CuO NPs/Al NPs samples suggest that synthesis of CuO NWs by thermal annealing is a simple and convenient way to produce nanostructured CuO for thermite reactions.

4. Conclusion

In summary, we have experimentally determined the exothermic onset temperatures and heat release characteristics of energetic CuO/Al core/shell NWs in inert He through DSC measurements. The synthesis of the NW thermites involves two simple steps: (1) growing CuO NWs by the thermal annealing of copper and (2) depositing a layer of Al by magnetron sputtering. The exothermic onset temperature of the core/shell NWs is about 100 °C below the melting temperature of Al and insensitive to the CuO/Al equivalence ratio, but it increases significantly with the heating rate. The CuO/Al core/shell NWs, comparing to conventional nano-thermites prepared by mixing NPs, has no endothermic peak associated with residual Al melting in the heat release profile and has significantly reduced activation energy for the thermite reaction between CuO and Al. These observations suggest the great potential of core/shell NW-based thermites due to their excellent spatial uniformity, ease of ignition, large reactivity and applicability to other material compounds.

Acknowledgments

Y.O. acknowledges support from the Japan Student Services Organization Fellowship. P.M.R. acknowledges support from the Link Foundation Energy Fellowship. X.L.Z. acknowledges support from the Powell Foundation at Stanford University. The authors sincerely thank Prof. Robert F. Feigelson at Stanford University for sharing the differential scanning calorimetry (DSC) and Dr. Romain Gaume for his technical support with the DSC measurements.

References

[1] K.K. Kuo, G.A. Risha, B.J. Evans, E. Boyer, *Mat. Res. Soc. Symp. Proc.* (2004) 3–14.
[2] L.L. Wang, Z.A. Munir, Y.M. Maximov, *J. Mater. Sci.* 28 (14) (1993) 3693–3708.
[3] R. Orru, M. Sannia, A. Cincotti, G. Cao, *Chem. Eng. Sci.* 54 (15–16) (1999) 3053–3061.
[4] C. Rossi, K. Zhang, D. Esteve, P. Alphonse, P. Tailhades, C. Vahlas, *J. Microelectromech. Sci.* 16 (4) (2007) 919–931.
[5] E.L. Dreizin, *Prog. Energ. Combust.* 35 (2) (2009) 141–167.
[6] D. Stamatis, Z. Jiang, V. Hoffmann, M. Schoenitz, E. Dreizin, *Combust. Sci. Technol.* 181 (1) (2009) 97–116.
[7] P.F. Pagoria, G.S. Lee, A.R. Mitchell, R.D. Schmidt, *Thermochim. Acta* 384 (1–2) (2002) 187–204.
[8] M.B. Talawar, R. Sivabalan, T. Mukundan, et al., *J. Hazard. Mater.* 161 (2–3) (2009) 589–607.
[9] M.L. Pantoya, J.J. Granier, *J. Therm. Anal. Calorim.* 85 (1) (2006) 37–43.
[10] J.J. Granier, M.L. Pantoya, *Combust. Flame* 138 (4) (2004) 373–383.
[11] K. Brandstadt, D.L. Frost, J.A. Kozinski, *Proc. Combust. Inst.* 32 (2009) 1913–1919.
[12] S.F. Son, B.W. Asay, T.J. Foley, R.A. Yetter, M.H. Wu, G.A. Risha, *J. Prop. Power* 23 (4) (2007) 715–721.
[13] B.S. Bockmon, M.L. Pantoya, S.F. Son, B.W. Asay, J.T. Mang, *J. Appl. Phys.* 98 (6) (2005) 064903/1–064903/7.
[14] C.E. Aumann, G.L. Skofronick, J.A. Martin, *J. Vac. Sci. Technol., B* 13 (3) (1995) 1178–1183.
[15] R.A. Yetter, G.A. Risha, S.F. Son, *Proc. Combust. Inst.* 32 (2009) 1819–1838.
[16] D.G. Kim, J. Kaneko, M. Sugamata, *J. Japn. Inst. Metals* 57 (11) (1993) 1325–1332.
[17] S. Umbrajkar, M.A. Trunov, M. Schoenitz, E.L. Dreizin, R. Broad, *Propell. Explos. Pyrot.* 32 (1) (2007) 32–41.
[18] S.M. Umbrajkar, M. Schoenitz, E.L. Dreizin, *Propell. Explos. Pyrot.* 31 (5) (2006) 382–389.
[19] M. Schoenitz, T.S. Ward, E.L. Dreizin, *Proc. Combust. Inst.* 30 (2005) 2071–2078.
[20] D.S. Moore, S.E. Son, B.W. Asay, *Propell. Explos. Pyrot.* 29 (2) (2004) 106–111.
[21] K.B. Plantier, M.L. Pantoya, A.E. Gash, *Combust. Flame* 140 (4) (2005) 299–309.
[22] D. Prentice, M.L. Pantoya, B.J. Clapsaddle, *J. Phys. Chem. B* 109 (43) (2005) 20180–20185.
[23] R. Shende, S. Subramanian, S. Hasan, et al., *Propell. Explos. Pyrot.* 33 (2) (2008) 122–130.
[24] S. Apperson, R.V. Shende, S. Subramanian, et al., *Appl. Phys. Lett.* 91 (24) (2007) 3.
[25] K.J. Blobaum, M.E. Reiss, J.M.P. Lawrence, T.P. Weihs, *J. Appl. Phys.* 94 (5) (2003) 2915–2922.
[26] J.D. Ferguson, K.J. Buechler, A.W. Weimer, S.M. George, *Powder Technol.* 156 (2–3) (2005) 154–163.
[27] V.E. Sanders, B.W. Asay, T.J. Foley, B.C. Tappan, A.N. Pacheco, S.F. Son, *J. Prop. Pow.* 23 (4) (2007) 707–714.
[28] D. Prentice, M.L. Pantoya, A.E. Gash, *Energ. Fuel.* 20 (6) (2006) 2370–2376.
[29] K.J. Blobaum, A.J. Wagner, J.M. Plitzko, D. Van Heerden, D.H. Fairbrother, T.P. Weihs, *J. Appl. Phys.* 94 (5) (2003) 2923–2929.
[30] K. Zhang, C. Rossi, G.A.A. Rodriguez, C. Tenailleau, P. Alphonse, *Appl. Phys. Lett.* 91 (11) (2007) 113117/1–113117/3.
[31] K.L. Zhang, C. Rossi, M. Petrantoni, N. Mauran, *J. Microelectromech. Sci.* 17 (4) (2008) 832–836.
[32] X. Jiang, T. Herricks, Y. Xia, *Nano Lett.* 2 (12) (2002) 1333–1338.
[33] O. Kubaschewski, C.B. Alcock, *Metall. Thermochem.*, Pergamon Press, London, 1979.
[34] S.M. Umbrajkar, M. Schoenitz, E.L. Dreizin, *Thermochim. Acta* 451 (1–2) (2006) 34–43.
[35] H.E. Kissinger, *Anal. Chem.* 29 (11) (1957) 1702–1706.
[36] C. Michaelsen, K. Barmak, T.P. Weihs, *J. Phys. D-Appl. Phys.* 30 (23) (1997) 3167–3186.

Combustion and Flame xxx (2011) xxx–xxx

Contents lists available at ScienceDirect

Combustion and Flame

journal homepage: www.elsevier.com/locate/combustflame

Flash ignition of Al nanoparticles: Mechanism and applications

Yuma Ohkura, Pratap M. Rao, Xiaolin Zheng *

Department of Mechanical Engineering, Stanford University, Stanford, CA 94305, USA

ARTICLE INFO

Article history:
Received 15 February 2011
Received in revised form 10 May 2011
Accepted 10 May 2011
Available online xxxx

Keywords:
Energetic material
Flash ignition
Melt dispersion mechanism
Aluminum
Nanoparticle

ABSTRACT

Aluminum nanoparticles (Al NPs), due to their high energy density, are important materials for propulsion systems, material synthesis and hydrogen generation. However, the oxidation mechanism of Al NPs at large heating rate remains inconclusive due to the lack of direct experimental evidence. Here, we studied the oxidation mechanism of Al NPs under large heating rate (on the order of 10^6 K/s or higher) by a simple flash ignition method, which uses a camera flash to ignite Al NPs. The flash ignition occurs when the Al NPs have suitable diameters and sufficient packing density to cause a temperature rise above their ignition temperatures. Importantly, transmission electron microscopy analysis reveals that the Al NPs are oxidized via the melt-dispersion mechanism, providing the first direct experimental evidence thereof. Finally, flash ignition is also applicable to the ignition of flammable gaseous, liquid and solid materials by the addition of Al NPs in lieu of sparks and hotwire igniters.

1. Introduction

Aluminum is an important fuel for various propulsion systems due to its large energy density (83.8 kJ/cm^3) [1], twice as high as that of gasoline (34.2 kJ/cm^3). For micron-sized Al particles, their combustion process is similar to that of liquid droplet combustion (d^2 law) [2] and the oxidation process occurs after the melting of the outer aluminum oxide. On the other hand, Al nanoparticles (NPs), comparing to micron-sized Al particles, have much lower ignition temperature (~900 K) [3,4], faster burning rates (~2400 m/s) [5] and have the potential to improve the performance of various propulsion systems. However, fundamentally, the oxidation mechanism of Al NPs is still a matter of debate. There are two theories to describe the oxidation process of Al NPs, (1) the diffusion oxidation mechanism (DOM) [6,7] and (2) the melt-dispersion mechanism (MDM) [8–11]. The DOM occurs when Al is heated with a slow heating rate, such that Al and oxygen diffuse towards each other through the growing oxide shell, which has been observed by TEM studies [6]. On the other hand, the MDM typically occurs at large heating rates (i.e., 10^6–10^8 K/s) [9], and postulates that the volume increase due to the melting of Al causes a build-up of large dynamic pressure within the NP. This high pressure ruptures the Al_2O_3 shell and generates an unloading pressure wave that propagates to the center of the particle and disperses the molten Al into small clusters at high velocity. Although the MDM has been proposed and studied analytically [8–12], direct TEM evidence has not been reported, to the best of our knowledge. Herein, we applied a flash ignition method [13–17] to Al NPs to study their oxidization behavior at high heating rates. We found that Al NPs are ignited by the melt-dispersion mechanism, which to the best of our knowledge, is the first direct experimental observation thereof. In addition, flash ignition is also applicable to the ignition of flammable gaseous, liquid and solid materials by the addition of Al NPs in lieu of sparks and hotwire igniters.

2. Experimental

Flash ignition of Al NPs is achieved by using a commercial camera flash (Vivitar 285 HV), which is equipped with a xenon lamp. The maximum energy density of the flash unit is estimated to be slightly above 620 mJ/cm^2 [15,18,19]. Specifically, tens of milligrams of Al NPs (d_{avg} = 60–96 nm, size distribution: 10–300 nm, see Supplementary material, SkySpring International Inc.) were placed on top of a 1 mm thick glass slide that was located 2 cm above the xenon flash tube in air. The Al NPs are ignited by a single exposure of the camera flash (Fig. 1a and b) and they burn in air for about 10 s with a yellow glow (Fig. 1b, inset). The Al NPs change from dark gray, loose powders to light gray aggregated particles after combustion (Fig. 2a). The original Al NPs are spherical and highly agglomerated with an average diameter in the range of 60–96 nm (Fig. 2b) with a 2 nm thick native aluminum oxide layer (Fig. 4a) and, after flash ignition, they are oxidized into much smaller NPs (3–20 nm, Fig. 5i), which are agglomerated (Fig. 2c). It was found that successful flash ignition is not sensitive to the mass of Al NPs in the range of 10–1000 mg. The flash ignition method can be applied to solid mixtures containing Al NPs, such as a

* Corresponding author. Address: Department of Mechanical Engineering, Stanford University, Bldg. 520, Rm. 520 J, Stanford, CA 94305, USA. Fax: +1 650 723 1748.
E-mail address: xlzheng@stanford.edu (X. Zheng).

0010-2180/$ - see front matter © 2011 The Combustion Institute. Published by Elsevier Inc. All rights reserved.
doi:10.1016/j.combustflame.2011.05.012

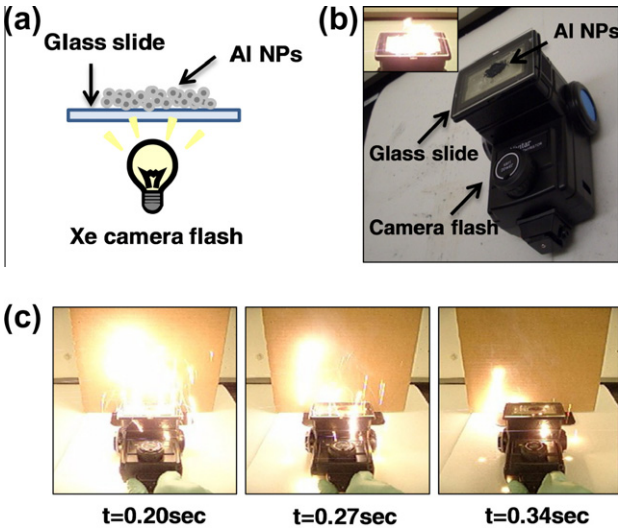

Fig. 1. Flash ignition of Al NPs and their thermite mixture with CuO NPs. (a) Schematic and (b) optical images of the experimental setup for ignition of Al NPs (d_{avg} = 60–96 nm) by a camera flash. Inset: photograph of the burning of flash ignited Al NPs which casts a yellow glow and lasts for about 10 s. (c) Photographs of the burning process of a thermite mixture of Al and CuO NPs ignited by a flash. (For interpretation of the references to color in this figure legend, the reader is referred to the web version of this article.)

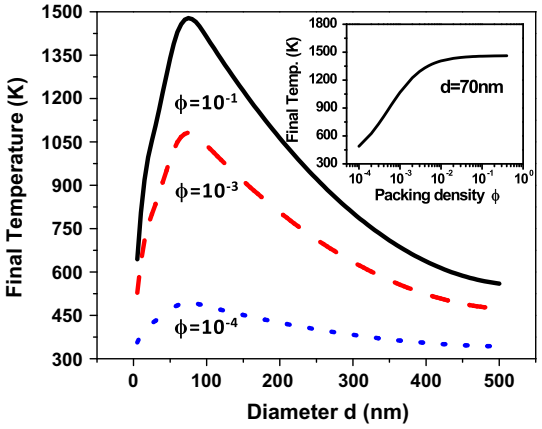

Fig. 3. Estimated temperature rise of Al particles by a flash exposure as a function of the Al particle diameter for different packing densities. The maximum temperature rise occurs at d = 75 nm. Inset: The temperature rise of Al NPs with a diameter of 70 nm as a function of the packing density of Al NPs. The final temperature rise of Al NPs with a diameter of 70 nm is less than 1 K for an isolated particle, but above 1100 K when the packing density is above 1%.

stoichiometric mixture of Al NPs and CuO NPs (d_{avg} = 60 nm, Inframat Advanced Materials). The thermite mixture was mixed by hand for 2 min and the degree of mixing was found not critical for the success of flash ignition. Once the Al ignites, the Al/CuO mixture reacts through the exothermic thermite reaction: $2Al + 3CuO \rightarrow Al_2O_3 + 3Cu$. The thermite reaction, in contrast to the burning of pure Al in air, proceeds violently and lasts less than a few seconds (Fig. 1c). Following the reaction, the color of the thermite mixture turns from black into brown, indicating the formation of copper (Fig. 2d). The melting of copper during the reaction causes the products of the thermite reaction to agglomerate into much larger, micron sized particles (Fig. 2f). Furthermore, the flash ignition method can be extended to the ignition of liquid and gaseous fuels (e.g., heptane, methane) by the addition of Al NPs (see Supplementary video) on condition that the particle surface is exposed to the oxidant (oxygen or metal oxide). In the case of heptane, a few drops of heptane (1 ml) were poured in a Buchner flask located 2 cm above the xenon flash tube, and the Buchner flask was connected to a pipette with 10 mg of Al NPs inside. The Al NPs were injected from the pipette to the flask and ignited subsequently by flash, which ignites heptanes at multiple locations. The ignition of heptane was accompanied by a pop sound, and kept burning until the heptane was consumed. For methane ignition, a mixture of methane and air was filled inside a one-side closed glass tube with an inner diameter of 35 mm and length of 16 cm. Al NPs (10 mg) were placed on top of the glass slide and the open-side of the glass tube was placed on top of a glass slide. Upon exposure to the flash, the methane/air mixture was ignited at the bottom by the Al NPs and a laminar flame propagated across the tube while the Al NPs was burning at the bottom of the tube. These experiments demonstrate a distributed optical ignition method that results in the ignition of solid phase energetic materials, liquid and gaseous fuels by the addition of Al NPs.

It should be noted that flash ignition of Al NPs was not observed when NPs were placed sparsely over the glass slide by drop casting Al NPs diluted with hexane onto the slide and then allowing the hexane to evaporate. Similarly, flash ignition of Al micron particles (d_{avg} = 20 μm, Sigma Aldrich) was not observed under any conditions. The results of the above experiments suggest that the packing density and the diameter of Al NPs are important factors for successful flash ignition.

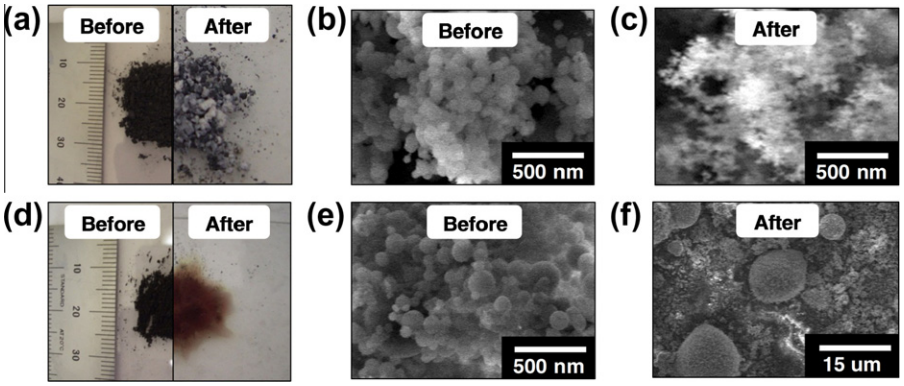

Fig. 2. Comparison of Al NPs and Al/CuO thermite mixture before and after exposure to the camera flash. (a–c) Optical and SEM images of Al NPs before and after the exposure. The original spherical Al NPs break up into smaller clusters after burning. (d–f) Optical and SEM images of Al–CuO NPs before and after the exposure. The products of the thermite reaction agglomerated into much larger, micron sized particles.

Please cite this article in press as: Y. Ohkura et al., Combust. Flame (2011), doi:10.1016/j.combustflame.2011.05.012

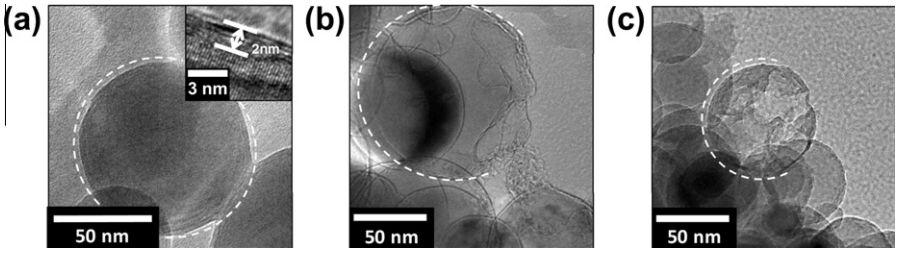

Fig. 4. Exposure of Al NPs to a flash in Ar. (a) TEM image of the Al NPs before flash exposure. Inset: the Al NP is covered by an alumina shell about 2 nm thick. (b and c) TEM images of two different sizes of Al NPs after flash exposure in Ar showing that both alumina shells have ruptured after the flash exposure.

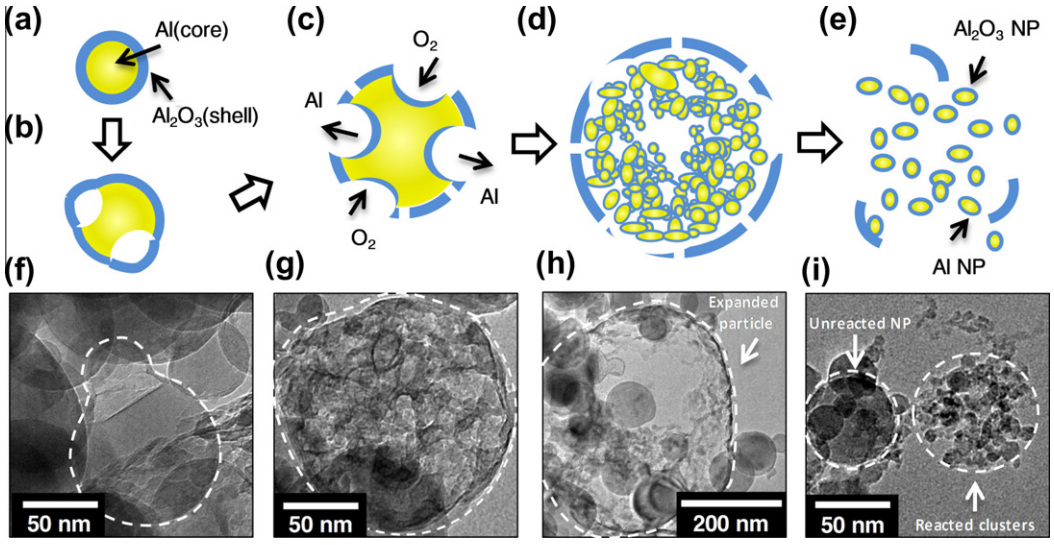

Fig. 5. Exposure of Al NPs to a flash in air and the melt-dispersion mechanism of Al oxidation. (a–e) Schematics and (f–i) TEM images illustrate the oxidation process of the Al NPs. (a) Initial Al NPs are covered by a Al_2O_3 shell. (b and f) Al melts upon rapid heating which pushes the shell outwardly. (c and g) The shell ruptures and the melted Al becomes in contact with air. (d and i) the large hollow sphere corresponds to the expanded Al NPs, where most Al has flown away from the particle center and been oxidized at the particle surface. (e and j) the hollow sphere fractures into small clusters of 3–20 nm in sizes. These clusters are consisted of both Al_2O_3 particles and partially oxidized Al particles.

3. Estimation of the temperature increase of single and multiple Al particles

To further investigate Al particle flash ignition, we estimated the temperature increase of Al particles by a single flash exposure. The flash ignition of Al NPs is achieved by the photo-thermal effect, when the energy of the incident light absorbed by Al NPs is sufficient to raise their temperatures beyond their ignition temperatures. The purpose of the calculation is to simulate the initial stage of flash ignition and to understand the qualitative dependence of temperature rise on the size and packing density of Al NPs.

3.1. Estimation of the temperature increase of single Al particles

First, we estimated the temperature rise from room temperature (300 K) of single isolated particles when exposed to a flash. The spectrum of the camera flash is assumed to be a blackbody radiation at a temperature of 6500 K [20] and the incident light intensity, I_{inc}, is approximately 1000 W/cm^2 on the basis of energy density of 1 J/cm^2 and the flash duration of 1 ms [15,21]. The light absorption by the Al_2O_3 shell is neglected, since Al_2O_3 is almost optically transparent [22]. Since Al has high thermal conductivity, the temperature distribution inside the Al particle is assumed to be constant. We estimated the temperature rise of Al particles by using the heat transfer equations of a single sphere of radius R embedded in homogeneous air, where the heat source term comes from the energy absorption rate of Al NPs by the incident flash light.

$$c_{p,\mathrm{Al}}\rho_{\mathrm{Al}}V_{\mathrm{Al}}\frac{\partial T_{\mathrm{Al}}(t)}{\partial t}+4\pi R^2 G[T_{\mathrm{Al}}(t)-T_{air}(t,r=R)]=P, \tag{1}$$

$$c_{p,air}\rho_{air}\frac{\partial T_{air}(t,r)}{\partial t}-K\nabla^2 T_{air}(t,r)=0, \tag{2}$$

and the boundary condition is

$$K\frac{\partial T_{air}(t,r)}{\partial r}\bigg|_{r=R}=G[T_{air}(t,r=R)-T_{Al}(t)], \tag{3}$$

where $c_{p,air}$, $c_{p,\mathrm{Al}}$, and ρ_{air}, ρ_{Al} are specific heat (J/kg K) and the density (kg/m^3) of air and Al respectively. V_{Al} is the volume of Al; R is the radius of the particle; G is the surface conductance between the Al particle and air (MW/m^2 K); P is the total energy absorption rate per particle (W), and K is the thermal conductivity of air (W/mK). A finite G represents a temperature discontinuity between the interface of the particle and air. Solving for the above equations, in the limit of $t\to\infty$, the maximum temperature rise of a single particle is [21,23]

$$\Delta T_{\mathrm{Al,max}}=\frac{P}{4\pi R^2}\left(\frac{1}{G}+\frac{R}{K}\right), \tag{4}$$

where $\Delta T_{Al,max}$ is the maximum temperature increase of the particle. Although the surface conductance G between the particles and air can vary from 10 to 1000 MW/m^2 K [24], the corresponding final temperature only differs by 0.1 K. Hence, we neglected the contribution of G to the temperature rise in Eq. (4). P is the total energy absorption rate per particle (W), which is calculated by integrating over the specific energy absorption rate over all the wavelengths λ, ranging from 185 to 2000 nm and corrected with the emissivity factor ($\varepsilon = I_{inc}/\sigma T^4$), as shown in

$$P = \frac{I_{Inc.}}{\sigma T^4}\int \frac{1}{\lambda^5}\frac{4\pi^2 c^2 \hbar}{\exp[2\pi c\hbar/(\lambda k_B T)]-1} C_{abs}(\lambda)d\lambda, \quad (5)$$

where σ is the Stefan–Boltzmann constant; c is the speed of light; $\hbar$ is the reduced Planck constant, and k_B is the Boltzman constant. The specific energy absorption rate at a specific wavelength is the product of the absorption cross-section, $C_{abs}(\lambda)$, and the intensity of the incident light at the wavelength. The absorption cross-section $C_{abs}(\lambda)$ was calculated by using a Mie theory calculator "Mieplot" [25].

The estimated temperature rises of single Al particles with diameters of 70 nm and 20 μm are 0.18 K and 197 K respectively, and both final temperatures are much lower than the typical ignition temperature of Al NPs, which ranges from about 833 K to the melting point of Al (933 K) [26–28]. This result is consistent with our experimental observation that sparsely dispersed Al NPs and micron-sized particles are not ignited by a camera flash.

3.2. Estimation of the temperature increase of multiple Al particles

Hence, it is necessary to consider the effect of multiple Al particles, for which we define the packing density as $\phi = V_{Al}/V_{air}$, i.e., the volume ratio of Al particles to the confined air among the particles. The temperature rise of Al particles was estimated by assuming that the energy absorbed by the Al particles is used to heat up the particles and the confined air.

$$(\rho_{air}V_{air}c_{p,air} + \rho_{Al}V_{Al}c_{p,Al})\Delta T = pV_{Al}\Delta t, \quad (6)$$

$$\Delta T = \frac{p\Delta t}{\frac{\rho_{air}c_{p,air}}{\phi} + \rho_{Al}c_{p,Al}}, \quad (7)$$

where p is the energy absorption rate per unit volume (W/m^3) by Al, and Δt is the flash duration (s). Here for estimation purpose, we assumed that the Al and air have the same temperature rise, although the actual temperature of Al will be higher than that of air [29]. We also neglected the optical interactions among Al particles and the possible air expansion between Al NPs due to the heating. It should be noted that the estimation presented here is not a rigorous flash heating model, which is far from trivial due to the complexity in describing the Al NP distribution and interfacial heat conductivity, but rather its purpose is to provide qualitative information on the dependence of temperature rise on the size and packing density of Al NPs.

Figure 3 shows the dependence of the temperature rise of the Al particles on their sizes and packing densities. First, the largest temperature rise is expected for NPs with approximately 75 nm diameter, regardless of the packing density. As the size of the Al particles increases beyond 75 nm, the temperature rise decreases because the particles scatter more and absorb less energy. In addition, larger micron Al particles require much higher ignition temperature of above 1200 K [26]. Hence, Al μPs cannot be ignited by a flash. Second, there is a critical Al packing density to achieve flash ignition because, for Al particles of the same diameter, their temperature rise increases sharply with the Al packing density and eventually saturates when the packing density is roughly above 1% (Fig. 3, inset). The reason that higher temperature rise is expected for larger packing densities of Al particles in that more heat per unit volume is absorbed. In summary, successful flash ignition of Al NPs relies on two important parameters: their diameters and their packing densities. Finally, it should be noted that the absorption cross section of Al NPs peaks at different wavelengths for Al NPs of different diameters [30], so it is desirable for the light source to have a broad spectrum emission to ignite Al NPs, which unavoidably have different diameters. For this reason, flash light is more advantageous than lasers for igniting Al NPs.

4. Al NP oxidation mechanism

Next, we investigated the oxidation mechanism of Al NPs ignited by a camera flash. Al NPs ignited by the flash are likely to be oxidized by the MDM due to the large heating rate, on the order of 10^6 K/s or higher. To verify the MDM oxidation, Al NPs were first exposed to the flash in an inert Ar gas to avoid further oxidation. Al NPs (10 mg) were placed inside a Buchner flask filled with argon gas. The xenon flash tube was placed 2 cm below the Buchner flask. The flash was triggered ten times with an interval of 10 s. During the flash exposure, no ignition was observed and the remaining Al NPs were collected for TEM characterization. The TEM images (Fig. 4a and inset) show that Al NPs have average diameters of 60–96 nm and roughly 2 nm thick Al_2O_3 shells before the flash exposure. After the flash exposure, the Al_2O_3 shell is partially ruptured and the molten Al is dispersed out of the shell (Fig. 4b and c). The observation suggests that the flash provided enough energy to melt the Al and generated a large dynamic pressure inside the NP to rupture its shell, and eventually led to the outflow of the molten Al.

We further studied the oxidation process of Al NPs in air by examining multiple NPs after the flash exposure using TEM. Due to the intrinsic spatial non-uniformity of the flash light intensity and the packing density of Al NPs, Al NPs will have different temperature rise and exposure to oxygen, so their oxidation process will quench at different stages after the flash exposure. Therefore, by examining many Al NPs, we can re-construct the oxidation process of Al NPs as illustrated in Fig. 5. Initially, similar to the case in Ar, Al melts upon exposure to the flash, which pushes the oxide shell outwards (Fig. 5b and f). When the pressure rise associated with the melting of Al is large enough, it ruptures certain regions of the oxide shell and the molten Al flows out (Fig. 5c and g). Subsequently, Al and oxygen contact with each other and react exothermically. The heat generated further causes more Al to melt or even evaporate, which pushes the oxide shell further out, and the original Al NP has grown from less than 100 nm to over 300 nm in diameter (Fig. 5d and h). As shown in Fig. 5h, the big hollow sphere corresponds to the expanded Al particle. Eventually, the entire particle fractures and breaks into clusters of 3–20 nm, much smaller than the original Al NPs (Fig. 5e and i). The clusters consist of both Al_2O_3 particles and partially oxidized Al particles. These observations strongly suggest that the Al NPs ignited by the flash are oxidized by the MDM.

5. Conclusions

In summary, we have demonstrated that Al NPs can be ignited by a camera flash through the photo-thermal effect. Flash ignition has the advantages of low power input, multi-point initiation and broad spectrum emission. Our analysis reveals that successful flash ignition requires Al NPs to have a suitable submicron diameter range and a large packing density, in order to achieve sufficient temperature rise. Furthermore, TEM analysis of Al NPs after the flash exposure in Ar and air suggests that Al NPs are oxidized

through the MDM, which is the first direct experimental observation thereof. The flash ignition of Al NPs may find uses in many engineering applications requiring distributed, nonintrusive and miniaturizable ignition, and is applicable to the ignition of flammable gaseous, liquid and solid materials by the addition of Al NPs in lieu of sparks and hotwire igniters.

Acknowledgments

This work was supported by the Army Research Office under the Grant W911NF-10-1-0106. Y.O. acknowledges support from the Japan Student Services Organization Fellowship. P.M.R. acknowledges support from the Link Foundation Energy Fellowship.

Appendix A. Supplementary material

Supplementary data associated with this article can be found, in the online version, at doi:10.1016/j.combustflame.2011.05.012.

References

[1] M.C.G.S.H. Fischer, in: Proc. 24th Int. Pyrotechnics Seminar, Monterey, CA, 1998, pp. 1–6.
[2] M.W. Beckstead, Intern. Aerodynamics Solid Rocket Propul. (2004) 1–46.
[3] C.J.T.P. Parr, D. Hanson-Parr, K. Higa, K. Wilson, in: 39th JANNAF Combustion Subcommittee Meeting, 2003.
[4] T.T.K.C.J. Bulian, J.A. Puszynski, in: 31st International Pyrotechnics Seminar, Fort Collins, CO, 2004.
[5] R. Shende, S. Subramanian, S. Hasan, S. Apperson, R. Thiruvengadathan, K. Gangopadhyay, S. Gangopadhyay, P. Redner, D. Kapoor, S. Nicolich, W. Balas, Propellants, Explos., Pyrotech. 33 (2) (2008) 122–130.
[6] A. Rai, K. Park, L. Zhou, M.R. Zachariah, Combust. Theory Modell. 10 (5) (2006) 843–859.
[7] S. Chowdhury, K. Sullivan, N. Piekiel, L. Zhou, M.R. Zachariah, J. Phys. Chem. C 114 (20) (2010) 9191–9195.
[8] V.I. Levitas, B.W. Asay, S.F. Son, M. Pantoya, Appl. Phys. Lett. 89 (7) (2006).
[9] V.I. Levitas, B.W. Asay, S.F. Son, M. Pantoya, J. Appl. Phys. 101 (8) (2007).
[10] V.I. Levitas, Combust. Flame 156 (2) (2009) 543–546.
[11] V.I. Levitas, M.L. Pantoya, K.W. Watson, Appl. Phys. Lett. 92 (20) (2008).
[12] V.I. Levitas, M.L. Pantoya, B. Dikici, Appl. Phys. Lett. 92 (1) (2008).
[13] P.M. Ajayan, M. Terrones, A. de la Guardia, V. Huc, N. Grobert, B.Q. Wei, H. Lezec, G. Ramanath, T.W. Ebbesen, Science 296 (5568) (2002) 705.
[14] N. Wang, B.D. Yao, Y.F. Chan, X.Y. Zhang, Nano Lett. 3 (4) (2003) 475–477.
[15] L.J. Cote, R. Cruz-Silva, J.X. Huang, J. Am. Chem. Soc. 131 (31) (2009) 11027–11032.
[16] M.R. Manaa, A.R. Mitchell, R.G. Garza, P.F. Pagoria, B.E. Watkins, J. Am. Chem. Soc. 127 (40) (2005) 13786–13787.
[17] A.M. Berkowitz, M.A. Oehlschlaeger, Proc. Combust. Inst. 33 (2011) 3359–3366.
[18] B. Chehroudi, S.A. Danczyk, C. Morgan, A. Badakhshan, in: JANNAF 6th MSS/4th LPS/3rd SPS Joint Meeting, 2008.
[19] The energy density was estimated by the camera flash unit guide number, where Vivitar 285HV and 730 AFN have 120 and 115 (ISO100/ft.) @50 mm, respectively.
[20] H.K. Aslin, Rev. Sci. Instrum. 38 (3) (1967) 377–381.
[21] N. Zeng, A.B. Murphy, Nanotechnology 20 (37) (2009) 375702.
[22] Y.A. Akimov, W.S. Koh, Nanotechnology 21 (23) (2010) 235201.
[23] H.H. Richardson, M.T. Carlson, P.J. Tandler, P. Hernandez, A.O. Govorov, Nano Lett. 9 (3) (2009) 1139–1146.
[24] D.G. Cahill, W.K. Ford, K.E. Goodson, G.D. Mahan, A. Majumdar, H.J. Maris, R. Merlin, S.R. Phillpot, J. Appl. Phys. 93 (2) (2003) 793–818.
[25] P. Laven, MiePlot v4.2 Software. <www.philiplaven.com/MiePlot.htm>.
[26] M.A. Trunov, M. Schoenitz, E.L. Dreizin, Propellants, Explos., Pyrotech. 30 (1) (2005) 36–43.
[27] E.L. Dreizin, Prog. Energy Combust. Sci. 35 (2) (2009) 141–167.
[28] R.A. Yetter, G.A. Risha, S.F. Son, Proc. Combust. Inst. 32 (2009) 1819–1838.
[29] A.O. Govorov, H.H. Richardson, Nano Today 2 (1) (2007) 30–38.
[30] M.H. Chowdhury, K. Ray, S.K. Gray, J. Pond, J.R. Lakowicz, Anal. Chem. 81 (4) (2009) 1397–1403.

Supplementary Information for

Flash Ignition of Al Nanoparticles: Mechanism and Applications

Yuma Ohkura, Pratap M. Rao, and Xiaolin Zheng*

Department of Mechanical Engineering, Stanford University, Stanford, CA 94305

1. Size distribution of Al NPs

The size distribution of Al NPs shown in Table 1 is provided by SkySpring Nanomaterials.

Table 1: Size distribution of Al NPs

Size interval (nm)	Mass Fraction %
10-18	12.9
18-36	13.5
36-60	16.6
60-96	18.0
96-140	13.5
140-200	12.5
200-300	13.0

Reducing minimum flash ignition energy of Al microparticles by addition of WO_3 nanoparticles

Yuma Ohkura, Pratap M. Rao, In Sun Cho, and Xiaolin Zheng[a)]
Department of Mechanical Engineering, Stanford University, Stanford, California 94305, USA

(Received 13 November 2012; accepted 18 January 2013; published online 30 January 2013)

Aluminum (Al) is an attractive solid fuel for rocket propulsion and energy conversion systems due to its large volumetric energy density, earth abundance, and low cost. Nonintrusive optical flash ignition is attractive for many applications due to its simplicity and flexibility in controlling the area exposed to the flash. However, flash ignition of Al microparticles (MPs) is challenging due to their higher minimum flash ignition energy, which originates from weaker light absorption and higher ignition temperature compared to Al nanoparticles (NPs). Herein, the minimum flash ignition energy of Al MPs is reduced by the addition of WO_3 NPs. © *2013 American Institute of Physics*. [http://dx.doi.org/10.1063/1.4790152]

Aluminum (Al), due to its large volumetric energy density of 83.8 kJ/cm^3,[1] is an important fuel for solid rocket propulsion,[2,3] high temperature processing,[4] and microelectromechanical systems (MEMS). For example, small amounts of Al are integrated into MEMS to generate heat, microthrusts, and gases for actuation and power supply.[5–8] However, a reliable and optical ignition method is desirable for practical utilization of Al fuel. Especially for MEMS applications, the small Al quantity and feature size impose a challenge for reliable ignition with common ignition methods requiring physical contact, such as hotwires, heaters, and piezoelectronic igniters.[9] Optical ignition by flash, instead, is very attractive because it works without physical contact and can easily achieve distributed ignition at multiple locations, thereby increasing reliability of ignition and flexibility of design. Optical flashes have been used to ignite Al nanoparticles (NPs) and many other nanomaterials, including carbon nanotubes, silicon nanowires, and graphene oxide.[10–14] In all these cases, the flash heats up the nanomaterials to temperatures beyond their ignition temperatures by the photothermal effect, leading to ignition. Compared to Al NPs, Al microparticles (MPs) are more suitable for practical systems since they are cheaper, safer to handle, and contain much higher Al content due to the much smaller fraction of dead volume and weight of the inert Al_2O_3 shell. Nevertheless, it is difficult to ignite Al MPs by flash due to their low light absorption and high ignition temperature, and ignition is only possible with a large flash energy (>1 J/cm^2 from a xenon flash lamp). Previous work on the combustion of Al MPs has shown that Al MPs burn much faster with the addition of nanoscale metal oxides.[15] Herein, we investigate the effect of adding WO_3 NPs on the flash ignition of Al MPs. We observe that the minimum flash ignition energy of Al MPs is greatly reduced by adding WO_3 NPs because WO_3 NPs improve both oxygen supply and light absorption from the flash.

Mixtures of Al MPs and WO_3 NPs are prepared by ultra-sonication using dimethylformamide (DMF) as a solvent. To study the efficacy of WO_3 NP-assisted flash ignition on Al MPs of different sizes, two different sizes of Al MPs, i.e., 2.3 μm (Atlantic Equipment Engineers) and 0.9 μm (Sigma-Aldrich) are separately mixed with WO_3 NPs. Al MPs and WO_3 NPs (80 nm, SkySpring Nanomaterials, Inc) are each weighed to satisfy the targeted fuel/oxidizer equivalence ratio while keeping a total mass of 0.530 g. The Al MP and WO_3 NP mixture is added to 10 ml of DMF and sonicated for 15 min to ensure uniform mixing. After sonication, the mixture is gently dried on a hotplate at 100 °C for 6 h to remove the DMF. Finally, the dried mixture powder is passed through a 140 mesh (105 μm) sieve to break up large agglomerates. The Al-to-WO_3 equivalence ratio (ϕ) and normalized equivalence ratio (ϕ_n) of the mixture are defined in the following equation:

$$\phi = \frac{\left(\frac{m_{Al}}{m_{WO3}}\right)}{\left(\frac{m_{Al}}{m_{WO3}}\right)_{st}}, \quad \phi_n = \frac{\phi}{1+\phi}, \tag{1}$$

where m_{Al} and m_{WO3} refer to the mass of Al and WO_3, respectively, and the subscript *st* refers to the stoichiometric condition for the reaction $2Al + WO_3 \rightarrow Al_2O_3 + W$. Although the Al MPs are encapsulated by a native inert Al_2O_3 shell (2–5 nm), the active Al content is 97.5% for the small (0.9 μm) and 99.0% for large (2.3 μm) Al MPs with a 5 nm shell. Hence, we assume that the entire mass of the Al MPs is Al when calculating the equivalence ratios.

A schematic of the flash ignition experimental setup is shown in Figure 1(a). Flash ignition of the mixture of Al MPs and WO_3 NPs is achieved by a commercial camera flash (AlienBees™ B1600 Flash Unit) equipped with a xenon ring lamp with a maximum areal flash energy density up to 0.84 J/cm^2 per flash. The areal energy density of the flash at each power setting is measured using an optical power detector (XLP12-3S-H2, Gentec-EO USA, Inc). The mixture of Al MPs and WO_3 NPs is placed on top of a 1 mm thick glass slide that is placed directly above the xenon ring lamp. For each flash ignition experiment, the mixture powder is gently packed into a cylindrical shape (diameter: 6.8 mm, height: 2.6 mm) to maintain the same volume and cross-section area exposed to the flash (Fig. 1(b)). To measure the minimum

a)Author to whom correspondence should be addressed. Electronic mail: xlzheng@stanford.edu.

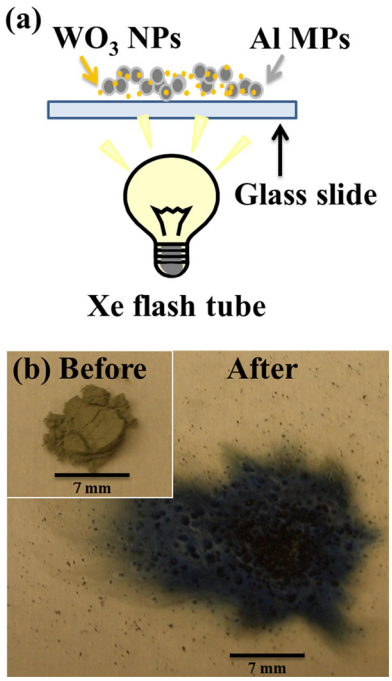

FIG. 1. Flash ignition of Al MPs with addition of WO_3 NPs. (a) Schematic of the experimental setup for ignition of a mixture of Al MPs (2.3 μm) and WO_3 NPs (80 nm) by a xenon flash. (b) Optical images of a mixture of Al MPs and WO_3 NPs ($\phi = 1$, $\phi_n = 0.5$) before and after the xenon flash exposure.

flash ignition energy, the power of the flash is increased gradually until flash ignition occurs. Flash ignition experiments are carried out both in air and in N_2 atmospheres. For the flash ignition experiments in N_2, the entire flash unit and samples are placed inside an inflatable polyethylene glove box (Atmosbag glove bag, Sigma-Aldrich) that is purged constantly with 99.95% pure N_2.

The wavelength-dependent light absorption properties of various mixture samples are obtained with an integrating sphere using a xenon lamp coupled to a monochromator (Model QEX7, PV Measurements, Inc.). For the reflectance (R%) measurement, the samples are mounted at the backside of the integrating sphere and the reflectance spectra are normalized to the reflection of a white-standard. The transmittance spectra (T%) are obtained by comparing the transmittance of test samples with a calibrated Si reference photodiode. Since the scattering component is not separately counted in the measurement, the absorption (A%) and scattering (S%) are calculated with the formula, $(A + S)\% = 100\% - T\% - R\%$.

Optical images in Figure 1(b) show the sample appearance before (inset) and after the flash ignition in air, where the sample is a stoichiometric mixture of Al MPs (2.3 μm) and WO_3 NPs (80 nm) with $\phi = 1$. After ignition, the mixture color changes from gray to dark blue. The dark blue color indicates that some WO_3 (yellow) is reduced to WO_{3-x} (blue), and not completely to W (silver or gray color). The sample is spread out over a larger area after ignition, suggesting a violent reaction that is accompanied with gas expansion. Before flash ignition, scanning electron microscope (SEM, FEI XL30 Sirion, 5 kV) images (Fig. 2(a)) show that the spherical Al MPs (2.3 μm) and the WO_3 NPs are mixed, forming a densely packed powder. After the flash

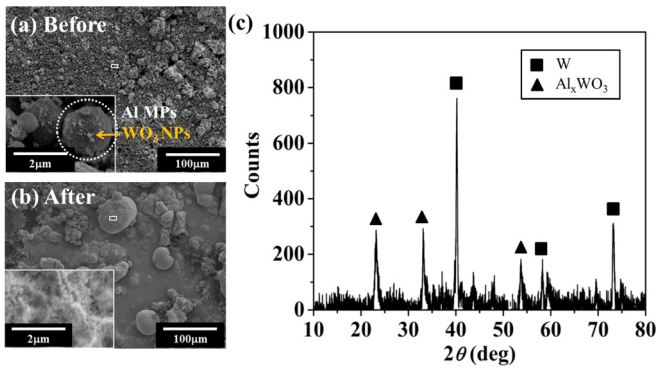

FIG. 2. Comparison of SEM images of a mixture Al MPs (2.3 μm) and WO_3 NPs (80 nm, $\phi = 1$, $\phi_n = 0.5$). (a) Before and (b) after the xenon flash exposure. Insets: enlarged view of the corresponding product surface. (c) X-ray diffraction pattern of the mixture of Al MPs and WO_3 NPs after ignition.

ignition, the products form much larger particles that are tens of microns in size (Fig. 2(b)), suggesting that melting and fusion occur together with reaction. These micron-sized particles are further analyzed by X-ray diffraction (XRD, PANalytical XPert 2, Cu Kα, 45 kV, 40 mA); the dominant peaks of the XRD pattern (Fig. 2(c)) are those of W and Al_xWO_3, indicating that WO_3 has been reduced and some portion of it has formed aluminum-tungsten bronze. The absence of WO_{3-x} and Al_2O_3 peaks in the XRD pattern is likely because they are either amorphous or poorly crystalline. All these characterizations confirm that reaction has occurred between Al MPs and WO_3 NPs upon exposure to a single optical flash. Flash ignition occurs when the energy of the incident light absorbed by the mixture of Al MPs/WO_3 NPs is sufficient to raise the mixture temperature beyond its ignition temperature.

WO_3 NPs influence the flash ignition of Al MPs in two ways: (i) increasing light absorption and (ii) decreasing ignition temperature by supplying oxygen to Al. To quantify the effect of WO_3 NPs, the minimum flash ignition energy (E_{min}) for the mixture of Al MPs and WO_3 NPs is plotted as a function of normalized Al/WO_3 equivalence ratio in both air (black squares) and inert N_2 (red circles) in Figure 3. Figures 3(a) and 3(b) correspond to larger Al MPs (2.3 μm) and smaller Al MPs (0.9 μm), respectively. The error bars are established by performing three experiments with identical conditions, and represent the range of measured E_{min} within the three measurements. First, both E_{min} curves (Figs. 3(a) and 3(b)) show a concave shape, with higher E_{min} values in both the Al lean and rich regions, a trend that is very similar to that of E_{min} for ignition of various gaseous fuel/air mixtures.[16] The lowest point of the E_{min} curve does not correspond to the stoichiometric condition of reaction $2Al + WO_3 \rightarrow Al_2O_3 + W$ ($\phi = 1$, $\phi_n = 0.5$), since WO_3 is not completely reduced to tungsten in the flash experiment. Second, when Al is the deficient species with respect to WO_3 ($\phi_n < 0.5$), E_{min} in air is comparable to that in N_2. The fact that E_{min} does not increase when gaseous O_2 is removed suggests that Al MPs are preferentially oxidized by the WO_3 NPs. WO_3 NPs are more effective oxidizers than air because of their large contact area with the Al MPs, which facilitates ignition through the diffusion-based reactive sintering mechanism.[17,18] Third, adding WO_3 NPs to pure Al MPs ($\phi_n = 1$)

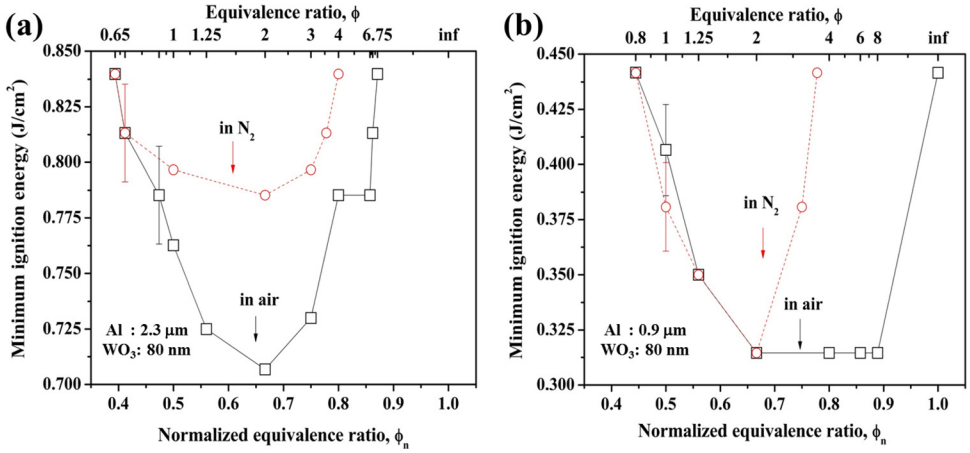

FIG. 3. Minimum flash ignition energy of Al MPs with addition of WO_3 NPs. (a) Large Al MPs (2.3 μm) and (b) small Al MPs (0.9 μm) mixed with WO_3 NPs with respect to normalized equivalence ratios in air and nitrogen gas.

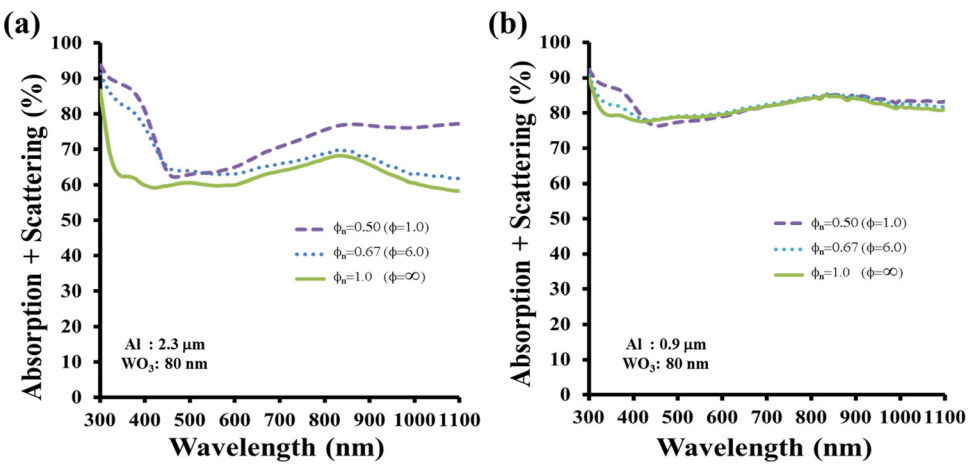

FIG. 4. Optical characterizations of Al MPs with addition of WO_3 NPs. Absorption plus scattering of (a) large Al MPs (2.3 μm) and (b) small Al MPs (0.9 μm) mixed with WO_3 NPs with respect to normalized equivalence ratios over the wavelength of 300–1100 nm.

or to Al MPs in excess supply with respect to WO_3 ($\phi_n > 0.5$), i.e., changing ϕ_n from 1 to 0.5, significantly lowers E_{min} because WO_3 oxidizes Al more effectively than air. Finally, when comparing Al MPs of two different sizes, E_{min} for the 2.3 μm Al MPs is on average 0.4 J/cm^2 higher than that for the 0.9 μm Al MPs, which is consistent with the reported observation of higher ignition temperature of 1600 K for larger (2.3 μm) particles compared to 1400 K for smaller (0.9 μm) particles.[19,20] Nevertheless, addition of WO_3 NPs reduces E_{min} for Al MPs of both sizes.

The above E_{min} measurements show that WO_3 NPs are more effective oxidizers than air for Al MPs. In addition, WO_3 NPs can also enhance the light absorption of the mixture of Al MPs/WO_3 NPs upon flash exposure, which can increase the temperature rise due to the photothermal effect. Figure 4 shows the light absorption spectra of several mixtures of Al MPs and WO_3 NPs over wavelengths of 300–1100 nm. Figures 4(a) and 4(b) correspond to larger (2.3 μm) and smaller (0.9 μm) Al MPs, respectively. First, for pure Al MPs ($\phi_n = 1.0$), the slight absorption increase around 830 nm corresponds to the interband transition frequency of 1.5 eV for aluminum.[21] For all the other samples containing WO_3 NPs, light absorption is clearly increased for wavelengths below 460 nm, consistent with the WO_3 bandgap of 2.7 eV ($\lambda = 460$ nm). Second, the smaller Al MPs absorb about 15% more light than the larger Al MPs, facilitating the flash ignition process. Third, the total light absorption is calculated by integrating the product of the xenon flash spectrum and the absorption plus scattering spectrum over 300–1100 nm wavelengths. The total light absorption is increased by 12.2% and 1.4% for the larger (2.3 μm) and smaller (0.9 μm) Al MPs, respectively, when a stoichiometric quantity of WO_3 NPs ($\phi_n = 0.5$) is added to the pure Al MPs. Since the light absorption enhancement due to the addition of WO_3 NPs is negligible for the smaller Al MPs, the reduction in E_{min} is mainly attributed to effective oxygen supply by WO_3 NPs due to their intimate and large contact area with Al MPs. On the other hand, for larger Al MPs, the reduction of E_{min} by WO_3 addition results from both effective oxygen supply and enhanced light absorption.

We have studied the effect of WO_3 NP addition on the flash ignition of Al MPs of two different sizes by measurement of the minimum flash ignition energy, E_{min}. E_{min} is greatly reduced by the addition of WO_3 NPs for Al MPs of both sizes. For the smaller Al MPs, the reduction of E_{min} mainly comes from the more effective oxygen supply by WO_3 NPs than by air. For the larger Al MPs, the E_{min} reduction is due to the combined effects of effective oxygen supply and light absorption enhancement by WO_3 NPs. These results extend previous report in flash ignition of expensive and lower energy density Al NPs to inexpensive and higher energy density Al MPs.

This work was supported by the Army Research Office under the Grant No. W911NF-10-1-0106. Y.O. acknowledges the support from the Japan Student Services Organization Fellowship.

[1]S. H. Fischer and M. C. Grubelich, in Proceedings of 24th International Pyrotechnics Seminar, Monterey, California, USA, 1998.
[2]M. W. Beckstead, *A Summary of Aluminum Combustion*, presented at the RTO/VKI Special Course on "Internal Aerodynamics in Solid Rocket Propulsion," Rhode-Saint-Genese, Belgium, 27–31, May 2002, and published in RTO-EN-023.
[3]T. L. Pourpoint, T. D. Wood, M. A. Pfeil, J. Tsohas, and S. F. Son, Int. J. Aerosp. Eng. **2012**, 1.
[4]L. L. Wang, Z. A. Munir, and Y. M. Maximov, J. Mater. Sci. **28**(14), 3693 (1993).
[5]H. H. DiBiaso, B. A. English, and M. G. Allen, Sens. Actuators, A **111**(2–3), 260 (2004).
[6]K. L. Zhang, S. K. Chou, S. S. Ang, and X. S. Tang, Sens. Actuators, A **122**(1), 113 (2005).
[7]D. Teasdale, V. Milanovic, P. Chang, and K. S. J. Pister, Smart Mater. Struct. **10**(6), 1145 (2001).
[8]C. Rossi, K. Zhang, D. Esteve, P. Alphonse, P. Tailhades, and C. Vahlas, J. Microelectromech. Syst. **16**(4), 919 (2007).
[9]C. Rossi and D. Estève, Sens. Actuators, A **120**(2), 297 (2005).
[10]Y. Ohkura, P. M. Rao, and X. Zheng, Combust. Flame **158**(12), 2544 (2011).
[11]S. Gilje, S. Dubin, A. Badakhshan, J. Farrar, S. A. Danczyk, and R. B. Kaner, Adv. Mater. **22**(3), 419 (2010).
[12]P. M. Ajayan, M. Terrones, A. de la Guardia, V. Huc, N. Grobert, B. Q. Wei, H. Lezec, G. Ramanath, and T. W. Ebbesen, Science **296**(5568), 705 (2002).
[13]N. Wang, B. D. Yao, Y. F. Chan, and X. Y. Zhang, Nano Lett. **3**(4), 475 (2003).
[14]L. J. Cote, R. Cruz-Silva, and J. Huang, J. Am. Chem. Soc. **131**(31), 11027 (2009).
[15]M. R. Weismiller, J. Y. Malchi, J. G. Lee, R. A. Yetter, and T. J. Foley, Proc. Combust. Inst. **33**(2), 1989 (2011).
[16]B. Lewis and G. Von Elbe, *Combustion, Flames and Explosions of Gases*, 3rd ed. (Academic, New York, 1987).
[17]Y. Yang, Z. Sun, S. Wang, and D. D. Dlott, J. Phys. Chem. B **107**(19), 4485 (2003).
[18]E. V. Chernenko, L. F. Afanaseva, V. A. Lebedeva, and V. I. Rozenband, Combust., Explos. Shock Waves **24**(6), 639 (1988).
[19]M. A. Trunov, M. Schoenitz, and E. L. Dreizin, Combust. Theory Modell. **10**(4), 603 (2006).
[20]Y. Huang, G. A. Risha, V. Yang, and R. A. Yetter, Combust. Flame **156**(1), 5 (2009).
[21]C. F. Bohren and D. R. Huffman, *Absorption and Scattering of Light by Small Particles* (Wiley-VCH Verlag GmbH, Weinheim, Germany, 1998).

Flash Ignition of Freestanding Porous Silicon Film: Effects of Film Thickness and Porosity

Yuma Ohkura, Jeffrey M. Weisse, and Xiaolin Zheng*

Department of Mechanical Engineering, Stanford University, Stanford, CA 94305

Abstract

Porous silicon (Si) is a promising material with a wide range of photonic and pyrotechnic applications. Optical and pyrotechnic proprieties of porous Si have been reviewed, and various on-chip integrated nanoenergetics are demonstrated. However, the optical ignition behavior of the fundamental system, the freestanding porous Si film in the air without an additional oxidizer has not been reported. Here, we demonstrate that freestanding porous Si films can be distributedly ignited by a Xe flash. We conducted high speed camera imaging, energy-dispersive X-ray spectroscopy, X-ray diffraction, and thermogravimetric analysis to understand the flash ignition process. Our experiments and simulations reveal that the minimum flash ignition energies are sensitive to film thickness and porosity. These two parameters are critical for minimizing any safety concerns since the freestanding porous Si could accidently ignite at low power and for optimizing the possible energetic applications with the ability to control the ignition.

Keywords: Nanoenergetic, Porous, Silicon, Porosity, Ignition

Porous silicon (Si) is crystalline Si that contains nanosized pores and was accidently discovered by the Uhlirs at the Bell labs in the mid 1950s[1]. Porous Si attracted great attentions in the early 1990s because it was found to exhibit quantum confinement effects by Ulrich Gösele[2] and Leigh Canham[3], leading to bright red to orange luminescence at energies greater than the bandgap energy of bulk silicon (1.1 eV). In 2001, porous Si was found to explode at temperatures as low as 4.2 - 90 K in cryogenic oxygen by Kovalev *et al.*[4], sparking new wave of interests of using porous Si as nanoenergetic materials. In addition to high reactivity, porous Si has a large volumetric energy density (80.7 kJ/cm^3)[5], over two time higher than trinitrotoluene (TNT), and it can rapidly release energy with a reported burning rate up to 3050 m/s.[6-9] Moreover, porous Si can be conveniently integrated into Micro-Electro-Mechanical Systems (MEMS) such as accelerometers[8] and airbag initiators[10] to produce heat, gas, and control delivery pressures.[11] Hence, porous Si has emerged as a promising material for energetic and pyrotechnic applications and the basic properties of porous Si for pyrotechnic applications were thoroughly reviewed by Koch *et al*.[12] and Plessis.[13]

Understanding the ignition properties of porous Si is of great practical importance to reliably initiate controlled porous Si combustion and to prevent unwanted combustion of safety reasons. Various ignition methods, such as mechanical fracture[14], laser[15] and hotwire[16] have been applied initiate porous Si reactions. However, optical ignition with a broad band of wavelength light source, such as Xe flash light, has not been reported. Flash ignition is fundamentally interesting because it couples the unique optical properties of porous Si with its extraordinary chemical reactivity. Flash ignition is practically convenient because it is non-intrusive, low-cost and can achieve distributed ignition of energetic materials to enhance the energy release rates.[17-23] In this study, we report the first successful flash ignition of freestanding porous Si in ambient air and investigate the effects of film thickness and porosity on the minimum flash ignition energy (E_{min}) with combined experimental and numerical studies. We find that the E_{min} increases with increasing the film thickness and decreasing the film porosity. Furthermore, for film thicknesses above 30 μm, the increase in the porosity leads to a sharp decrease on the E_{min} and the increment of E_{min} become smaller as the film thickness increases.

The freestanding porous Si film is prepared by electrochemically etching Si wafers (p-type, 0.1 – 0.9 Ω.cm), followed by an electropolishing step to release the porous Si film. Specifically, the back of Si wafers is first deposited with a 200nm-thick aluminum (Al) film, followed by half an hour annealing at 400°C to form good electrical contact, and the Al film serves as an electrode for the following electrochemical etching step. The Al deposited Si wafer is then placed in a Teflon anodization cell (Fig. S1) filled with an ethanolic HF electrolyte solution (mixture of 48% HF and 100% ethanol). The concentration of the solution is varied among three volumetric ratios (HF:Ethanol = 1:0.5, 1:0.75, 1:1) to alter the porosity of the final porous Si film. A constant current of 50 mA/cm^2 is applied between the Al electrode on the back of the Si wafer and a platinum (Pt) counter electrode submerged in the ethanolic HF solution for 2 - 40 minutes to control the porous Si film thickness.[24, 25] Next, the etched porous Si film is detached from the Si wafer by increasing the current to 200 mA/cm^2 for 15 sec due to electropolishing.[26] Finally, the detached porous Si film is removed from the anodization cell and dried with a critical point dryer (Samdri-PVT-3B, tousimis) to prevent porous Si films from cracking.

The experimental setup for flash ignition of porous Si is schematically illustrated in Fig. 1a. The porous Si film (inset of Fig. 1a) is placed on top of a 1 mm thick glass slide directly above the xenon ring lamp of a commercial camera flash (AlienBees B1600 flash unit)[22] as

shown in Fig. 1b (left image). Once the flash is triggered, the porous Si film ignites, vertically rises, and burns violently in air in less than a second (right image of Fig. 1b, Movie S1). The dynamic flash ignition process of the freestanding porous Si film is recorded by a high speed camera (FASTCAM SA5, Photron USA, Inc) that is equipped with a macro lens for higher spatial and temporal resolution. The upper left image in Fig. 2 shows the unreacted porous Si film. Only about 0.46 msec after the porous Si film is exposed to the xenon flash, ignition is observed along the front edge of the film. At 0.56 msec, ignition has propagated from the front edge to the middle part of the film as evidenced by the observed fragmented film. At the same time, another ignition is initiated near the back edge of the film and it also propagates towards the middle of the film (Fig. 2, lower right image). Around 1.09 msec, , the porous Si film jumps off the underlying glass slide and burns violently in air (Fig. 1b, right image). It should be noted that nonuniform ignition for the porous Si film is due to the curvature of the film that leads to varying distance to the Xe lamp. To measure the minimum flash ignition energy (E_{min}), the areal energy density of the flash at each power setting is measured using an optical power detector (XLP12-3S-H2, Gentec-EO USA, Inc) and the E_{min} of each sample is determined by increasing the power of the flash until ignition occurs. The typical porous Si sample size for the E_{min} experiment is about 1 mm x1 mm, which is much smaller than the diameter of the xenon ring lamp (15 mm), so that the indecent light intensity on the entire sample can be approximately assumed to be uniform.

To determine the degree of oxidation after the flash ignition, the original porous Si (without exposure to xenon flash) and xenon flash exposed sample are analyzed with X-ray diffraction (XRD, PANalytical XPert 2, Cu Kα, 45 kV, 40 mA), scanning electron microscope equipped with energy-dispersive X-ray spectroscopy (SEM-EDS, JEOL JXA-733A, JEOL USA, Inc.) and thermogravimetric analysis (TGA, LABSYS evo, Setaram). The XRD spectra (Fig. 3a) show that the intensity of the Si (400) peak decreases after flash ignition, indicating that porous Si is initially crystalline as expected and is only partially oxidized after flash ignition. The Si (400) peak after flash ignition is also shifted and broadened after flash ignition (Fig. 3a, inset), indicating that the grain size of Si crystal is reduced and there is non-uniform strain distribution in the porous Si.[27] The XRD spectra do not exhibit any crystalline SiO_2 peaks so only amorphous SiO_2 phase is formed by the flash ignition. To further confirm that the porous Si is oxidized by the xenon flash, we expose one part of the porous Si film to the xenon flash and cover the other part with an aluminum plate to block the incident light. The SEM-EDS oxygen concentration elemental mapping image qualitatively shows that the oxygen concentration is increased in the region that has been exposed to flash (Fig. 3b). Finally, TGA, together with EDS, is used to quantitatively assess the extent of oxidation after the xenon flash exposure. The porous Si films (before and after flash ignition) were heated up with the heating rate of 10 ^{o}C/min to 1000 ^{o}C using the TGA in the air and the increase in mass difference was recorded. Both samples are oxidized to $SiO_{1.85}$ in the TGA, which was identified using the EDS analysis calibrated by the pure SiO_2 reference. By monitoring the mass gain difference from the two porous Si films (before and after flash ignition) to $SiO_{1.85}$, we quantified the amount of oxygen for before and after flash ignition of porous Si films. The initial composition before the xenon flash exposure was partially oxidized, $SiO_{0.127}$, and after the flash ignition, the final product is identified as $SiO_{0.264}$. All these characterizations indicate that porous Si is only partially oxidized after flash ignition in ambient air conditions.

An important parameter for practical application of flash ignition for porous Si is the minimum ignition energy (E_{min}). The mechanism of flash ignition is through the photothermal

effect. When the porous Si film absorbs enough light to raise its temperature beyond its ignition temperature, flash ignition occurs. The ignition temperature of the porous Si is about 300°C in the air,[12] at which the surface Si-H bonds of the freshly prepared porous Si breaks and the exposed Si atoms react with oxygen, leading to ignition.[4] Here, we investigate the dependence of E_{min} on controlling two parameters: 1) film thickness and 2) porosity, because both parameters affect the optical absorption,[3] thermal conductivity[28-30] and combustion properties[7] of porous Si. Freestanding porous Si films with different thickness and porosity are prepared by varying the electrochemical etching time and the HF concentration. The film thickness increases with increasing the etching time. The porosity increases with decreasing the HF/ethanol volume ratio[24] and the low/intermediate/high porosities porous Si films are respectively prepared by etchants with the HF/ethanol volume ratio of 1:0.5/1:0.75/1:1. It should be noted that porosity also increases with increasing the etching time, correspondingly the film thickness, hence, it is necessary to study the effect of porosity by comparing films of the same thickness. The E_{min} of freestanding porous Si films are plotted as functions of film thickness and porosity in Fig. 4 and the error bar represents the standard deviation of the E_{min}. It is clearly seen that the E_{min} increases with increasing the film thickness and decreasing the film porosity.

To understand the observed dependence of the E_{min} on the film thickness and porosity, we calculate the dynamic temperature profiles within the porous Si film due to a single flash exposure using the COMSOL Multiphysics™ software. Specifically, the numerical simulation schematic is set up on the basis of our experimental configuration (Fig. 1a) and it is consisted of a porous Si film on top of a 1 mm thick glass slide and a pulse of heat is supplied from the bottom of the glass slide (Fig. 5a). We assume that this is a one-dimensional time dependent heat transfer problem in solids. In addition, heat provided by the Xe lamp is mainly absorbed by the porous Si according to the Beer-Lambert Law, not by the glass slide due to its high transparency, and porous Si simultaneously loses heat to the bottom glass slide due to heat conduction and air due to natural convection. The incident xenon flash is simplified into a single wavelength light source at 450 nm, where the xenon flash intensity peaks. The single pulse output of the flash is modeled with a Gaussian shape time distribution.

$$I_o(t) = \frac{E}{\sqrt{2\pi}\tau} \exp\left[\frac{-(t-\tau)^2}{2\tau^2}\right], \quad (1)$$

where E is the incident energy density (J/m^2), and τ is set to be 0.5 msec to model the xenon pulse time. The spatial and temporal temperature profiles within the porous Si and glass are described by a one-dimensional unsteady heat transfer equation

$$\rho C_p \frac{\partial T}{\partial t} = \alpha(1-R) I_o(t) \exp(-\alpha z) + \frac{\partial}{\partial z}\left(k \frac{\partial T}{\partial z}\right), \quad (2)$$

where T is the temperature (K), and ρ, C_p, k, and α are the density (kg/m^3), specific heat (J/(kg·K)), thermal conductivity (W/(m·K)), and absorption coefficient (m^{-1}) at 450nm of the porous Si for $z \geq 0$ and glass slide for $z < 0$, respectively. Since the glass is almost transparent for the flash light, its α value is set to be zero. The $I_o(t)$ (W/m^2) is the output power density of the laser and R is the reflectivity of porous Si at 450nm and set to be 0.1. The density of the porous Si is expressed as $\rho_{p\text{-}Si}=\rho_{bulk\text{-}Si}(1 - porosity)$. [30] The initial and boundary conditions are expressed as:

$$T(z,t=0)=300K;\quad T(z=-1mm,t)=300K;\quad k\left.\frac{\partial T}{\partial t}\right|_{z=d}=h(300K-T),$$

(3)

where d (μm) is the total thickness of the porous Si film, and h is the convective heat transfer coefficient of ambient air (5 W/m^{2}K). In COMSOL, the temperature profiles of porous Si films are simulated using a time dependent study in the application mode Heat Transfer in Solids. The material parameters for the silica glass, bulk silicon, and air are obtained from the COMSOL material library. Physical properties and values of porous Si are referred from literature values, which are listed in the Supporting Information (Table S1).

A representative temperature history of the porous Si film is shown in Fig. 5b for which the film is specified with a thickness d of 20 μm, porosity of 70 %, and incident energy density E (Eq. 1) of 700 mJ/cm^2. Initially at time = 0 msec, the entire porous Si film is at room temperature (300K). Immediately after the flash pulse at time = 0.5 msec, the temperature at the bottom of the porous Si layer rises above 600 K, which is close to experimental reported ignition temperature (300^{o}C) of the porous Si in air. [12] The temperature decreases with increasing z since the amount of light absorption drops exponentially with distance. Once the flash pulse is over (time = 1.0 - 2.0 msec), the temperature of the porous Si starts to cool down to room temperature due to heat losses to both glass and air. For qualitative comparison purpose, we define ignition numerically as long as the peak temperature of the porous Si exceeds 600K.

Next, the calculated maximum temperature rise due to flash heating is plotted as functions of the porous Si film thickness and porosity (Fig. 6a). Here, the thickness and porosity have varied between 1 – 50 μm, and 50 – 70 %, and the energy input is fixed at 700 mJ/cm^2. Based on the simulation, the largest temperature rise is expected around 5 μm in thickness. As the thickness of the porous Si film increases beyond 5 μm, the maximum temperature decreases because of the large total heat capacity. Below 5 μm, the sample is too thin to absorb all the incident light, resulting in a decrease in the maximum temperature. Second, as the porosity increases, the maximum temperature increases due to the loss in the in the total heat capacity. By defining the ignition temperature at 600 K, one can determine the ignition threshold thickness of the porous Si film. As the porosity increases, the ignition threshold thicknesses also increase. Substantial differences in the maximum temperature are predicted by varying the film thickness and porosity, which implies that the E_{min} of the porous Si films are strong functions of film thickness and porosity.

Next, we revealed the dependence of the E_{min} on the thickness and porosity in Figure 6b. The plot is created by calculating the ignition threshold thicknesses at various incident energy levels with different porosities. The E_{min} plot draws the similar conclusion from maximum temperature rise plot in Figure 6a, where the E_{min} decrease as the sample thicknesses are reduced or porosities are increased. In addition, an important feature is illustrated as the porous Si film thickness increases from 30 μm to 50 μm, the effect of porosity becomes stronger and film thickness becomes weaker. For thick films, the increase in the porosity indicates a sharp decrease in the E_{min} and the increment of E_{min} become smaller as the film thickness increases. This trend is expected from the experimental data in Figure 4, where the slope becomes less steep as the film thickness increases from 30 μm to 50 μm. This trend occurs since the maximum temperature is located at the bottom of the porous Si surface and the additional increase in the thickness would weakly have less of an effect on the overall effective heating volume. The small change in the effective heating volume maintains the maximum temperature profile regardless of

the increase in film thickness, therefore, controlling the maximum temperature rise by varying the total heat capacity with porosity becomes effective.

We have demonstrated that freestanding porous Si films can be ignited by a xenon flash through the photo-thermal effect, which increases the sample temperature to above the ignition temperature. After the xenon flash exposure, we have confirmed that porous Si films are oxidized in the air without the addition of any strong oxidizers. Our experiment and simulation reveals that the E_{min} of porous Si films are sensitive to two parameters: film thickness and porosity. These two parameters are critical for minimizing any safety concerns since the freestanding porous Si could accidently ignite at low power (< 1 J/cm^2) and for optimizing the possible energetic applications with the ability to control the E_{min}. The flash ignition of porous Si may find uses in engineering applications requiring reliable and miniaturizable ignition materials, such as on-chip integration of micro-thrusters and self-destructive systems for with electronics.

Acknowledgments

This work was supported by the by the Army Research Office under the Grant No. W911NF-10-1-0106. Y.O. acknowledges support from the Japan Student Services Organization Fellowship.

Figure Captions

Figure 1: (a) Schematic of the experimental setup for ignition of freestanding porous Si film by a xenon flash. (b) Optical images of a freestanding porous Si film before and during the xenon flash exposure.

Figure 2: Ignition and oxidation propagation of freestanding porous Si film upon the xenon flash pulse. The porous Si film ignites from multiple locations and the oxidation propagates over the porous Si film.

Figure 3: (a) X-ray diffraction pattern of before and after the xenon flash exposure. Insets: enlarged view of (400) peaks where the peaks are shifted/broadened due to oxidation. (b) SEM-EDS oxygen elemental mapping image of porous Si film for un-exposure and exposed area to the xenon flash pulse.

Figure 4: Minimum flash ignition energies of freestanding porous Si film as a function of thickness for different porosities.

Figure 5: (a) Schematic of the simulation setup for estimating the temperature rise as a function of time of freestanding porous Si film by a xenon flash. (b) Estimated temperature profile within the freestanding porous Si film.

Figure 6: (a) Calculated maximum temperature rise of freestanding porous Si film by a xenon flash as a function of film thicknesses for different porosities. The ignition threshold thickness is determined at the ignition temperature of 600K. (b) Calculated minimum flash ignition energies of freestanding porous Si film as a function of porosity for different thicknesses.

References

1. Uhlir, A., Jr. *Bell System Technical Journal* **1956,** 35, (2), 333-347.
2. Lehmann, V.; Go□sele, U. *Applied Physics Letters* **1991,** 58, (8), 856.
3. Cullis, A. G.; Canham, L. T. *Nature* **1991,** 353, (6342), 335-338.
4. Kovalev, D.; Timoshenko, V.; Künzner, N.; Gross, E.; Koch, F. *Physical Review Letters* **2001,** 87, (6).
5. S. H. Fischer, M. C. G. *Proc. 24th Int. Pyrotechnics Seminar, Monterey, CA* **1998**, 1-6.
6. Plummer, A.; Kuznetsov, V.; Joyner, T.; Shapter, J.; Voelcker, N. H. *Small* **2011,** 7, (23), 3392-8.
7. Parimi, V. S.; Tadigadapa, S. A.; Yetter, R. A. *Journal of Micromechanics and Microengineering* **2012,** 22, (5), 055011.
8. Currano, L. J.; Churaman, W. A. *Journal of Microelectromechanical Systems* **2009,** 18, (4), 799-807.
9. Becker, C. R.; Apperson, S.; Morris, C. J.; Gangopadhyay, S.; Currano, L. J.; Churaman, W. A.; Stoldt, C. R. *Nano letters* **2011,** 11, (2), 803-7.
10. Clément, D.; Diener, J.; Gross, E.; Künzner, N.; Timoshenko, V. Y.; Kovalev, D. *physica status solidi (a)* **2005,** 202, (8), 1357-1364.
11. Rossi, C.; Zhang, K.; Esteve, D.; Alphonse, P.; Tailhades, P.; Vahlas, C. *Journal of Microelectromechanical Systems* **2007,** 16, (4), 919-931.
12. Koch, E.-C.; Clément, D. *Propellants, Explosives, Pyrotechnics* **2007,** 32, (3), 205-212.
13. du Plessis, M. *physica status solidi (c)* **2009,** 6, (7), 1763-1768.
14. Morris, C. J.; Laflin, K. E.; Churaman, W. A.; Becker, C. R.; Currano, L. J.; Gracias, D. H. **2012**, 1245-1248.
15. Kaierle, S.; Wang, S.; Shen, R.; Ye, Y.; Hu, Y.; Wu, L.; Yang, C.; Liu, J.; Cao, J. **2013,** 8796, 87960C-87960C-6.
16. Wang, S.; Shen, R.; Ye, Y.; Hu, Y. *Nanotechnology* **2012,** 23, (43), 435701.
17. Ajayan, P. M.; Terrones, M.; de la Guardia, A.; Huc, V.; Grobert, N.; Wei, B. Q.; Lezec, H.; Ramanath, G.; Ebbesen, T. W. *Science* **2002,** 296, (5568), 705.
18. Cote, L. J.; Cruz-Silva, R.; Huang, J. X. *Journal of the American Chemical Society* **2009,** 131, (31), 11027-11032.
19. Manaa, M. R.; Mitchell, A. R.; Garza, R. G.; Pagoria, P. F.; Watkins, B. E. *Journal of the American Chemical Society* **2005,** 127, (40), 13786-7.
20. Berkowitz, A. M.; Oehlschlaeger, M. A. *Proceedings of the Combustion Institute* **2010**, (In Press, Corrected Proof).
21. Wang, N.; Yao, B. D.; Chan, Y. F.; Zhang, X. Y. *Nano letters* **2003,** 3, (4), 475-477.
22. Ohkura, Y.; Rao, P. M.; Cho, I. S.; Zheng, X. *Applied Physics Letters* **2013,** 102, (4), 043108.
23. Ohkura, Y.; Rao, P. M.; Zheng, X. *Combustion and Flame* **2011,** 158, (12), 2544-2548.
24. Herino, R.; Bomchil, G.; Barla, K.; Bertrand, C.; Ginoux, J. L. *Journal of The Electrochemical Society* **1987,** 134, (8A), 1994-2000.
25. Smith, R. L.; Collins, S. D. *Journal of Applied Physics* **1992,** 71, (8), R1.
26. Cisneros, R.; Pfeiffer, H.; Wang, C. *Nanoscale Research Letters* **2010,** 5, (4), 686-691.
27. Pap, A. E.; Kordas, K.; Toth, G.; Levoska, J.; Uusimaki, A.; Vahakangas, J.; Leppavuori, S.; George, T. F. *Applied Physics Letters* **2005,** 86, (4), 041501.
28. Amato, G. *Optical Engineering* **1997,** 36, (2), 423.

29. Devi, J. M.; Jeyachandran, M.; Ramachandran, K. *e-Journal of Nondestructive Testing and Ultrasonics* **2006,** 11, (6).
30. Shen, Q.; Toyoda, T. *Review of Scientific Instruments* **2003,** 74, (1), 601.
31. Bansal, N. P.; Doremus, R. H., Handbook of Glass Properties. Elsevier.

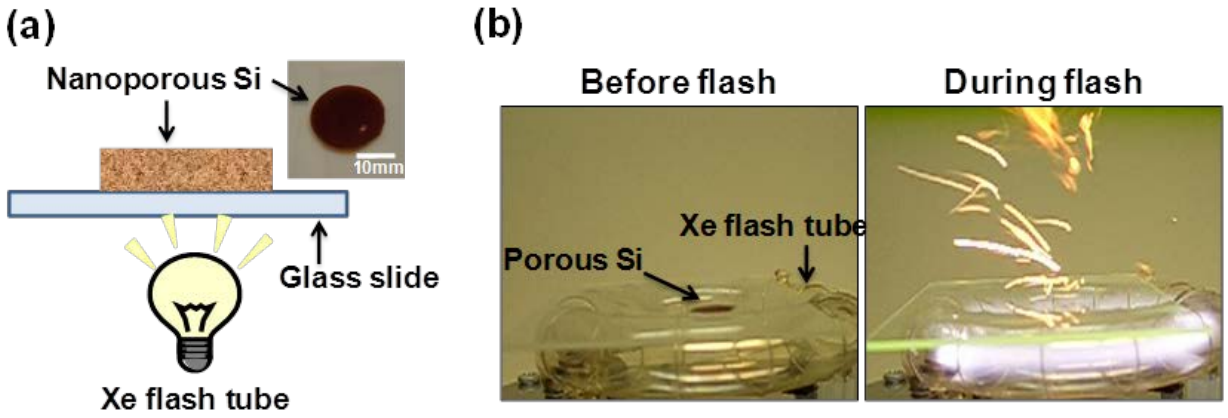
(a)
Nanoporous Si
10mm
Glass slide
Xe flash tube
(b)
Before flash
During flash
Xe flash tube
Porous Si

Figure 1

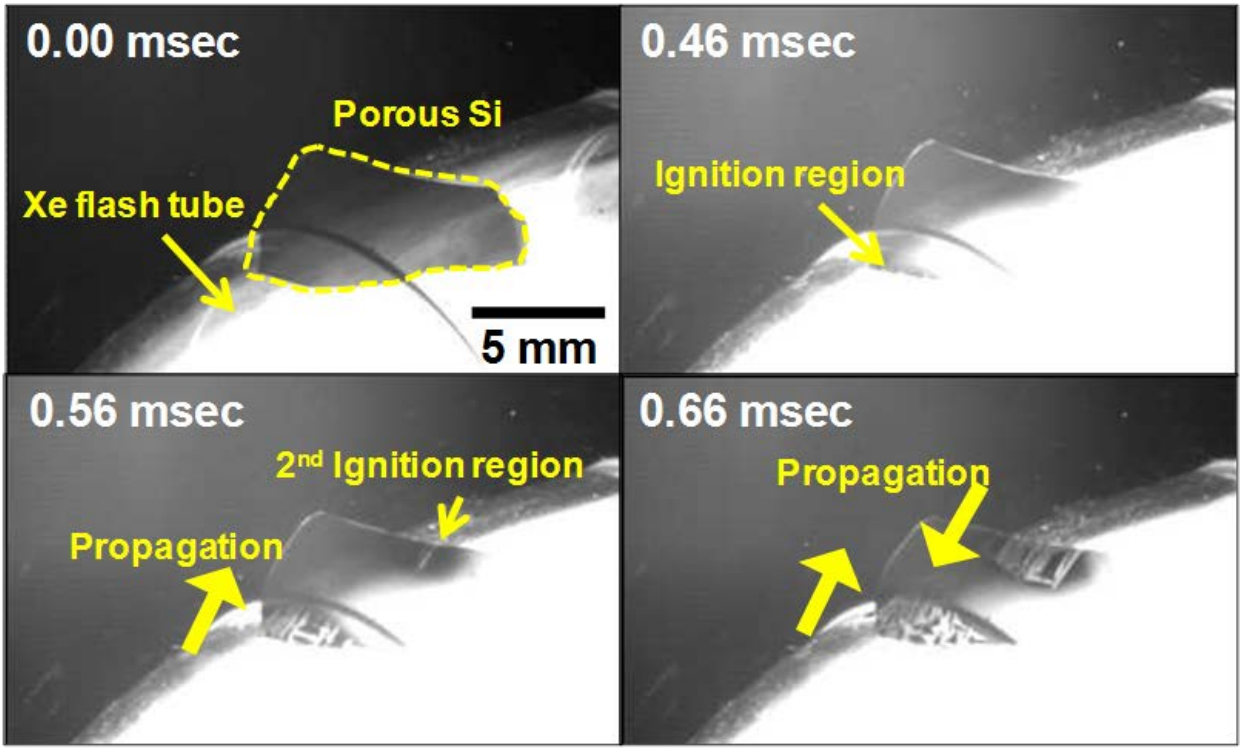
0.00 msec
Porous Si
Xe flash tube
5 mm
0.46 msec
Ignition region
0.56 msec
2nd Ignition region
Propagation
0.66 msec
Propagation

Figure 2

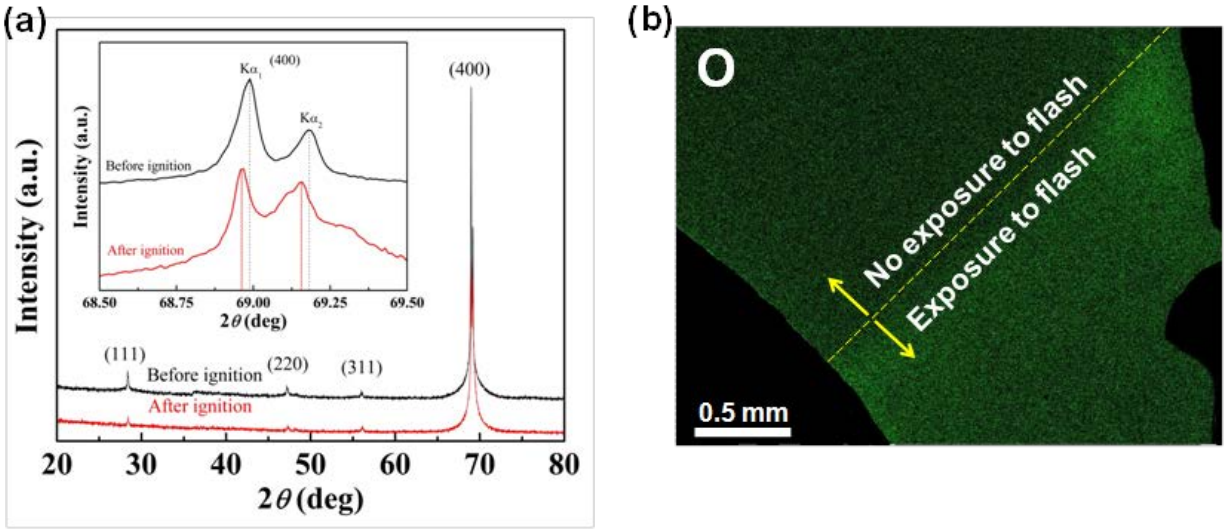
(a)
Intensity (a.u.)
Intensity (a.u.)
Kα1 (400)
Kα2
Before ignition
After ignition
68.50
68.75
69.00
69.25
69.50
2θ (deg)
(400)
(111)
Before ignition
(220)
(311)
After ignition
20
30
40
50
60
70
80
2θ (deg)
(b)
O
No exposure to flash
Exposure to flash
0.5 mm

Figure 3

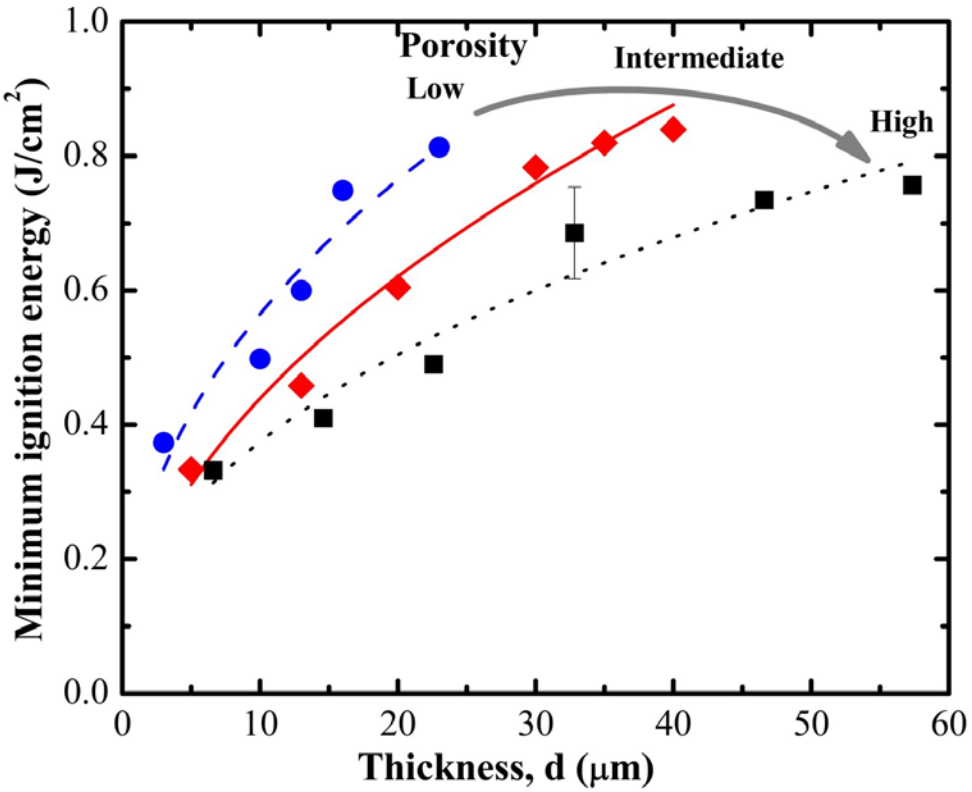
Porosity
Low
Intermediate
High
Minimum ignition energy (J/cm^2)
Thickness, d (μm)
1.0
0.8
0.6
0.4
0.2
0.0
0
10
20
30
40
50
60

Figure 4

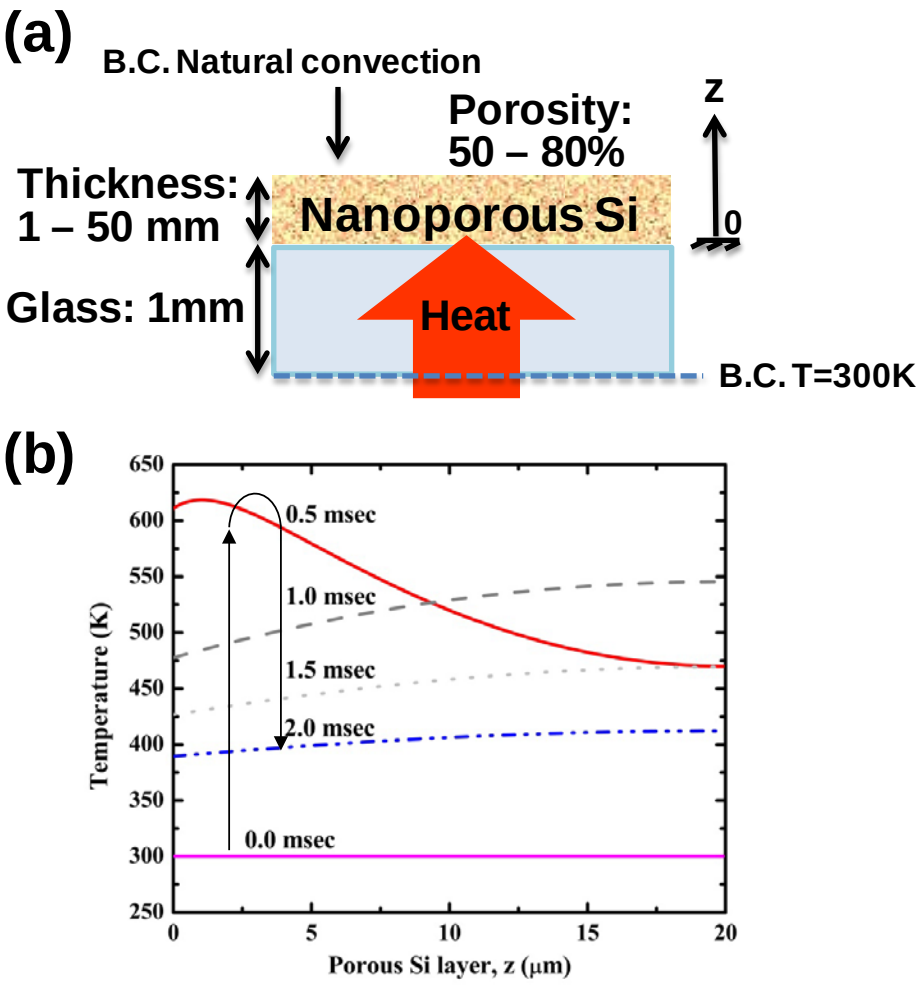
(a)
B.C. Natural convection
Porosity:
50 – 80%
z
Thickness:
1 – 50 mm
Nanoporous Si
0
Glass: 1mm
Heat
B.C. T=300K
(b)
Temperature (K)
650
600
550
500
450
400
350
300
250
0.5 msec
1.0 msec
1.5 msec
2.0 msec
0.0 msec
0
5
10
15
20
Porous Si layer, z (μm)

Figure 5

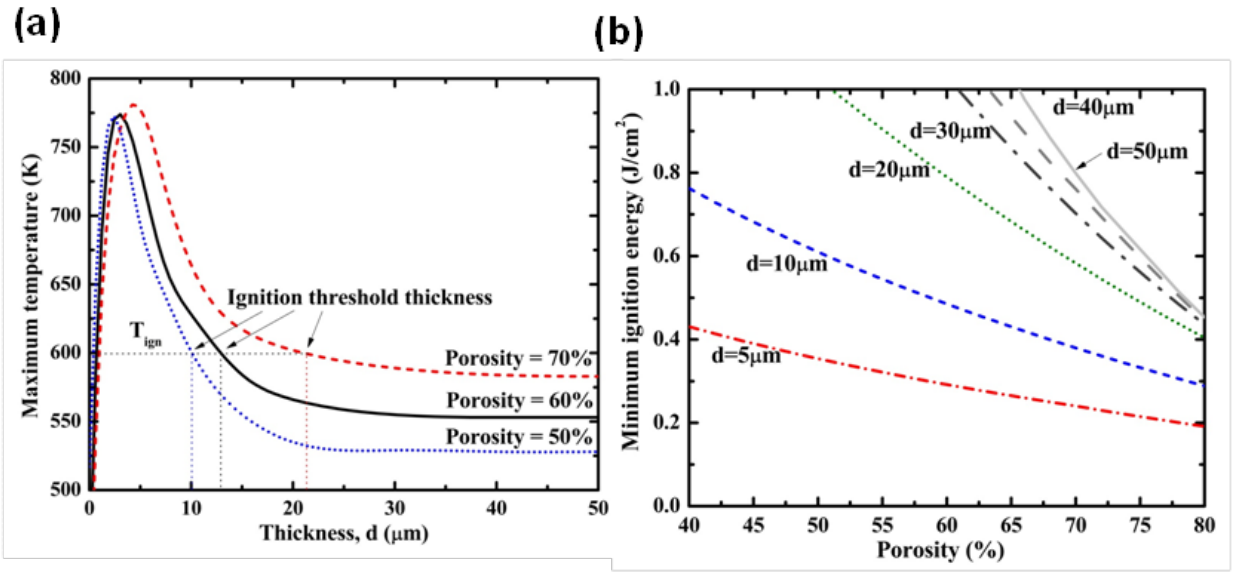
(a)
(b)
Maximum temperature (K)
Thickness, d (μm)
Ignition threshold thickness
T_ign
Porosity = 70%
Porosity = 60%
Porosity = 50%
Minimum ignition energy (J/cm²)
Porosity (%)
d=5μm
d=10μm
d=20μm
d=30μm
d=40μm
d=50μm

Figure 6